Pro gradu -tutkielma
Fysikaalisten tieteiden koulutusohjelma

Heat transfer in nanoscale colloids

Sampo Antero Saarinen
2014

Ohjaaja:	Ari Seppälä
Tarkastajat:	Kari Rummukainen
	Ari Seppälä

HELSINGIN YLIOPISTO
FYSIIKAN LAITOS

PL 64 (Gustaf Hällströmin katu 2)
00014 Helsingin yliopisto

HELSINGIN YLIOPISTO — HELSINGFORS UNIVERSITET — UNIVERSITY OF HELSINKI

Tiedekunta/Osasto — Fakultet/Sektion — Faculty	Laitos — Institution — Department
Faculty of Science	Department of Physics

Tekijä — Författare — Author
Sampo Saarinen

Työn nimi — Arbetets titel — Title

Heat transfer in nanoscale colloids

Oppiaine — Läroämne — Subject
Theoretical physics

Työn laji — Arbetets art — Level	Aika — Datum — Month and year	Sivumäärä — Sidoantal — Number of pages
pro gradu	March 2014	67

Tiivistelmä — Referat — Abstract

Nanofluids are a new class of colloids that is generally classified as solid particle suspensions such that the particle diameter is less than 100 nm. In the last decade they have exhibited anomalously high thermal conductivity compared to classical models. Additionally, nanoscale emulsions have shown similar behavior but have gathered less attention than solid particle nanofluids. The optimal preparation of nanoemulsions is not straightforward. Multiple factors have an effect on the final size distribution and therefore optimization is required.

Models for the anomalous behavior include effects of the Brownian motion, formation of particle clusters and ordering of liquid into a layer of high conductivity around the particles. In our measurements for nanoscale emulsions, we however observed no significant deviation from the classical models.

Besides conduction, nanofluids could also be utilized in convective heat transfer applications. The research on this field is more limited but indicates that increases in heat transfer exist also in convective transport. We perform heat transfer experiments on several n-decane in water nanoemulsions and nanoscale micelle colloids in the transition and turbulent flow regime.

Our results indicate that while the thermal properties of the samples were usually worse for convective applications than the reference, the heat transfer properties were similar or better especially at high Reynolds numbers.

Avainsanat — Nyckelord — Keywords
Nanofluid, Nanoemulsion, Heat transfer, Convection

Säilytyspaikka — Förvaringsställe — Where deposited

Muita tietoja — övriga uppgifter — Additional information

Contents

Symbols and abbreviations

Symbols

ϕ	Volume fraction
k_B	The Boltzmann constant
k	Thermal conductivity
α	Thermal diffusivity
T	Temperature
c_p	Specific heat
$\vec{q}$	Heat flux
ρ	Density
μ	Kinematic viscosity
ν	Dynamic viscosity
TEM	Transmission electron microscope
SEM	Scanning electron microscope
σ	Stefan-Boltzmann constant
h	The heat transfer coefficient

Chapter 1

Introduction

Heating and cooling systems are ubiquitous in many industries such as transportation, energy and electronics. The importance of the properties of the heat transfer medium is self-evident; its thermal and kinetic properties such as thermal conductivity and specific heat and viscosity determine the size and the efficiency of the system.

Most heat transfer systems utilize fluids as a transfer medium but thermal conductivity of most fluids is orders of magnitude lower than that of solids. For example, the thermal conductivity of water at room temperature is approximately 0.607 W/mK, whereas Copper features conductivity of 4002 W/mK [1]. It is a natural step to consider a fluid containing small metal particles to improve the conductivity of the base fluid; indeed, the theory of conduction in heterogeneous composites has been known since the work of Maxwell [2].

Recent advancements in technology have allowed creation of a new class of colloids, namely the suspensions of nanosized particles or nanofluids for short. Research in the last decade indicates that nanofluids exhibit far greater thermal conductivity enhancements than the classical theory would predict. Increases in conductivity have been observed even with minuscule particle loadings of less than 1 % volume. Furthermore, nanoscale colloids show far greater stability than micro sized particle suspensions. Since the year 2000, interest in nanofluids has increased nearly exponentially based on number of articles published as seen in figure 1.1. Recently, a few studies have also considered and reported similar enhancements in nanoemulsions [3][4][5]

The nature of thermal conduction in nanofluids is still unclear. Keblinski et al. [7] outlined four mechanism responsible for anomalous increase in thermal conductivity: particle clustering, Brownian motion of the particles, ordering of the liquid to form a high conductivity layer near the particles and ballistic heat transfer in the particles. However, it has also been proposed

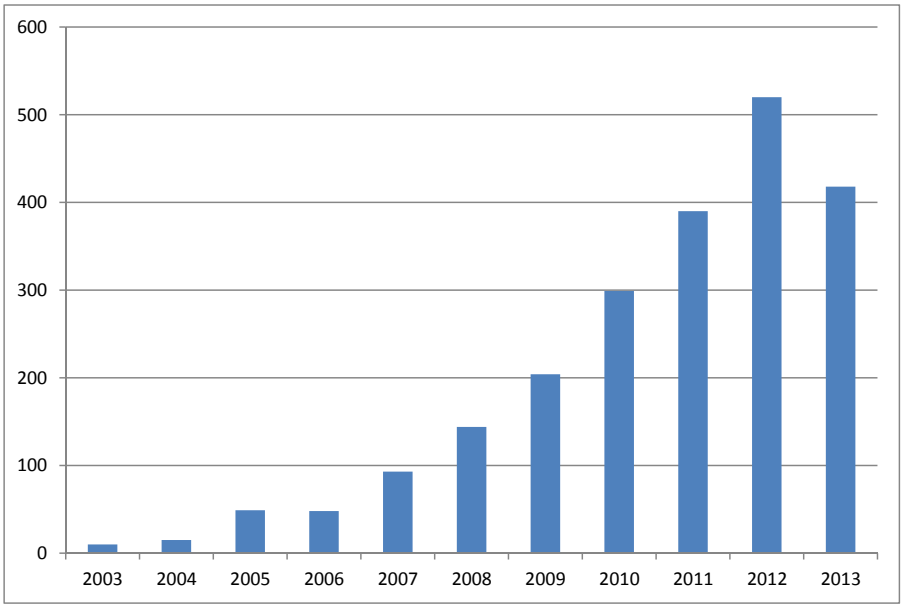

Figure 1.1: The number of articles with "nanofluid" in the topic has increased exponentially in the recent years [6]. Values were obtained 20.09.2013.

that the well established effective medium theories are adequate to explain the experimentally observed effects [8].

The goal of this thesis is to consider heat transfer in nanoscale colloids from both theoretical and experimental point of view. In chapter 2 we review and assess the validity of various models claimed to explain the phenomenon. However, for most applications, the important factor is the convective heat transfer. Chapter 3 concisely reviews classical theory of pipe flow and considers effects nanoparticles have on the heat transfer.

In addition to the literature review, this thesis has an experimental part. We consider convective heat transfer properties of nanoemulsions and suspensions of micelles. Chapter 4 explains the experimental methods and in chapter 5 the results are presented. Chapter 6 presents discussion on the findings and the conclusions.

Chapter 2

Thermal conduction in nanofluids

A definitive and widely accepted theory of thermal conduction in nanofluids has not yet been formulated. Macroscopic theories of thermal conduction in two component systems are well known and date back to Maxwell's work on electric conductivity of heterogeneous dielectrics [2]. Recent experiments however show higher conductivity enhancement than these theories predict. A few mechanism have been proposed, namely ballistic conduction in suspended particles, liquid ordering near the particles, clustering of particles and Brownian motion of the particles [7] [9] [10]. We will discuss each proposition in detail and consider other possible explanations such as the upper bound of macroscopic theory.

2.1 The heat equation

Thermal and electrical conductivity are mathematically similar phenomena. To illustrate this similarity, we briefly consider the heat equation and its derivation. Fourier's law concerning diffusive conduction of heat in a medium is [11]

$$\vec{q} = -k\nabla T, \tag{2.1}$$

where $\vec{q}$ is the heat flux, k the heat conductivity and T the temperature of the medium. To clearly see the connection between Maxwell's work on electrical conduction and thermal conductivity, we concisely review the derivation of the heat equation.

To justify the use of models for combinations of dielectrics, we will briefly discuss the heat equation. It can be derived by considering the change of total heat in an region A. Let $T(x,t)$ be the temperature in position x at

time t. The total heat in the region is thus

$$H(t) = \int_A c_p \rho T(x,t) dx \tag{2.2}$$

where c_p is the specific heat and ρ the density of the matter. The change in total heat is thus

$$\frac{dH(t)}{dt} = \int_A c_p \rho \frac{\partial T(x,t)}{\partial t} dx. \tag{2.3}$$

The only change in the heat happens through the boundary of the region and thus $\partial_t T = \alpha \nabla T$, where α is the thermal diffusivity $\alpha = k/c_p\rho$, and thus

$$\frac{dH(t)}{dt} = \int_{\partial A} k \nabla T(x,t) \cdot \vec{n} dS, \tag{2.4}$$

where $\vec{n}$ is a normal unit vector of the surface and dS is the surface element. Equating (2.3) and (2.4) and using the divergence theorem

$$\int_{\partial B} f \cdot \vec{n} dS = \int_B \nabla \cdot f dx \tag{2.5}$$

we find

$$\int_A c_p \rho \frac{\partial T(x,t)}{\partial t} dx = \int_A \nabla \cdot (k \nabla T(x,t))\, dx \tag{2.6}$$

and thus

$$c_p \rho \frac{\partial T(x,t)}{\partial t} = k \nabla^2 T(x,t) \tag{2.7}$$

which is

$$\frac{\partial T(x,t)}{\partial t} - \alpha \nabla^2 T(x,t) = 0, \tag{2.8}$$

which for the steady-state situation reduces to the Laplace equation $\nabla^2 \phi = 0$ meaning that discussion for electric potentials is equally valid for thermal diffusion.

2.2 Effective medium theories

Effective medium theory is a blanket name for models which represent the composite matter as homogeneous bulk matter, the effective conductivity of which is derived from the properties and configuration of the constituents without considering microscopic effects. The first effective medium theory for conductivity in heterogeneous matter was proposed by Maxwell [2] for dielectric consisting of bulk matter with conductivity k_f and well dispersed spheres with conductivity k_p. The subscripts are chosen for later clarity such that f correspond to the base fluid and p to the particle or the droplet. These

subscripts are used throughout the text unless otherwise noted. As noted in the earlier section, Maxwell's solution is also valid for thermal conduction as it is. The solution is

$$k_{eff} = k_f \left[\frac{k_p + 2k_f - 2\phi(k_f - k_p)}{k_p + 2k_f + \phi(k_f - k_p)} \right], \tag{2.9}$$

where ϕ is the volume fraction of the dispersed phase.

The outline of the derivation of the relation is as follows. Consider n small spheres of radius r_1 and conductivity k_p in a medium of conductivity k_f. Assuming all of the spheres are contained in a larger sphere of radius a, the potential at distance r from the sphere using solid harmonics expansion is

$$V = (Ar + nB\frac{1}{r^2})\cos\,\theta, \tag{2.10}$$

where B can be expressed as

$$B = \frac{k_p - k_f}{2k_p + k_f} a^3 A. \tag{2.11}$$

Now, consider a sphere made of material with conductivity K and radius a' such that the potential at distance r from the sphere is the same as (2.10). The potential is

$$V' = \left(Ar + a'^3 \frac{K - k_f}{2K + k_f} A \frac{1}{r^2} \right) \cos\,\theta. \tag{2.12}$$

Consider a situation where $a = a'$. It immediately follows that $V' = V$ and thus we need to have

$$a^3 \frac{K - k_f}{2K + k_f} = n a^3 \frac{k_p - k_f}{2k_p + k_f}, \tag{2.13}$$

from which the Maxwell's model follows with simple algebra and K is to be understood as the effective conductivity of the medium k_eff.

2.2.1 Modifications to the Maxwell's equation

Maxwell's solution, while useful, falls short when considering nanoscale colloids since it only takes into account the bulk properties of the constituents and the volume fraction of particles and ignores any effects such as particle size or shape. A group of thermal conductivity models can be classified as modifications to the Maxwell's equation that alleviate some of these shortcomings.

Based on Maxwell's solution, Hamilton and Crosser [12] formulated a modified solution to account for different particle shapes. The solution according to Hamilton-Crosser theory (HC) is

$$k_{HC} = k_f \left[\frac{k_p + (n-1)k_f - (\Psi - 1)\phi(k_f - k_p)}{k_p + (\Psi - 1)k_f + \phi(k_f - k_p)} \right], \tag{2.14}$$

where k_f and k_p are conductivities of the fluid and the particles respectively, ϕ is the particle volume fraction and Ψ is the empirical shape factor. For spherical particles, the equation reduces to Maxwell's original solution (2.9).

Another commonly encountered modification is the Maxwell-Garnett-model [13] for a medium consisting of a matrix medium ε_m and inclusions ε_i. It has been mostly used for composites of solids. The effective dielectric constant is

$$\varepsilon_{eff} = \varepsilon_m \frac{2(1-\phi)\varepsilon_m + (1+2\phi)\varepsilon_i}{(2+\phi)\varepsilon_m + (1-\phi)\varepsilon_i} \tag{2.15}$$

However, even modified effective medium theories do not take into account the microscopic phenomena such as Brownian motion or interaction between particles.

2.2.2 Hashin-Strikman bounds

The Hashin-Strikman (HS) bounds [14] are upper and lower limits of thermal conductivity enhancement predicted only by knowledge of the properties of the constituents and the volume fraction of the dispersed phase. The bounds are

$$k_- = k_f \left(1 + \frac{3\phi(k_p - k_f)}{3k_f + (1-\phi)(k_p - k_f)} \right), \tag{2.16}$$

and the upper bound is

$$k_+ = k_p \left(1 - \frac{3(1-\phi)(k_p - k_f)}{3k_p - \phi(k_p - k_f)} \right). \tag{2.17}$$

The lower limit corresponds to well dispersed particles, i.e. the Maxwell's model and the upper bound corresponds to a configuration in which the particles form linked chains surrounded by large areas of fluid. Multiple instances of thermal conductivity experiments fit within the HS bounds[8]. Chain forming agglomeration is discussed in more detail in section 2.5, but it should be noted that the assumptions underlying in the upper bound are very optimistic, especially for a fluid in motion, requiring the linked particles to be parallel to the direction of the heat flow. Furthermore, the claim sparked a correction[15] claiming that the data analysis by the authors of the original

proposition is faulty on a few of the data sets and that they ignored contrary evidence to formation of cluster, i.e. that thermal conductivity increases proportionally to the sonication time that is when nanoparticles are more dispersed [16].

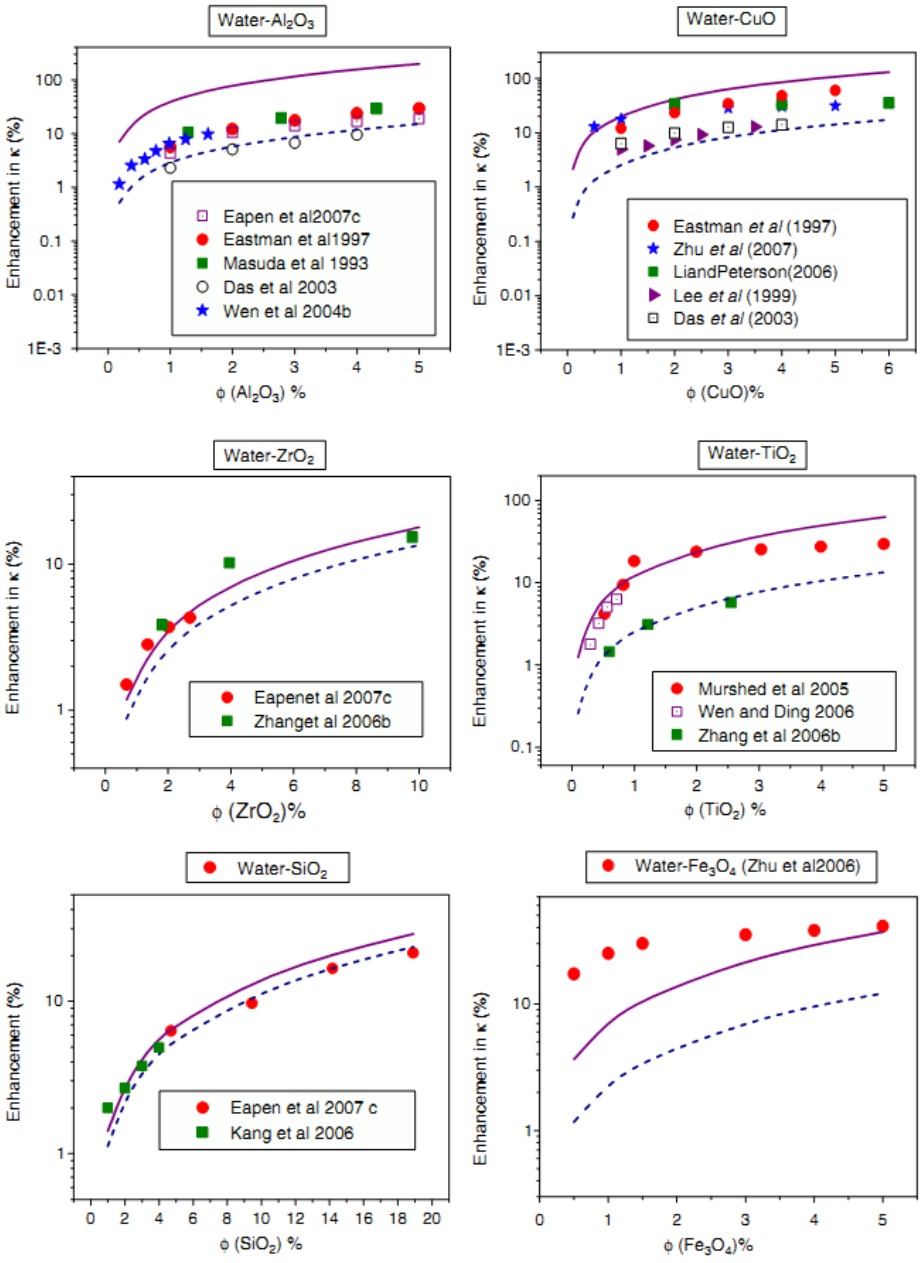

Figure 2.1: The figure is from [8]. The data is from [17],[18],[19], [20],[21],[22], [23],[24],[25],[26], [27]. Multiple instances of nanofluid thermal conductivity data seem to fit within the Hashin-Strikman bounds.

2.3 Ballistic heat transfer in particles

In macroscopic theories it is assumed that thermal conduction in materials is diffusive, i.e. governed by Fourier's law of conduction (2.1). As heat is carried by phonons in crystalline solids. In the solid, phonons are created at random and they scatter from defects and also from each other. Therefore, at long length scales, the assumption of diffusive thermal conduction is justified. Since the effects that cause "diffusive" transfer are probabilistic in nature, it is possible, that for short distances, the phonons move without significant resistance from scattering, i.e. they move ballistically. This significantly increases the heat flux through the medium and at the Casimir limit, the heat flux between two plates of temperatures T_1 and T_2 is

$$q_{Casimir} = \sigma(T_1^4 - T_2^4), \tag{2.18}$$

where σ is the Stefan-Boltzman constant.

The length scale where ballistic heat transfer is significant can be estimated from the mean free path of a phonon in a solid, that is [28]

$$l = \frac{10aT_m}{\gamma T}, \tag{2.19}$$

where a is the lattice constant, T_m the melting point of the substance, γ the Grüneisen parameter and T the temperature. For example, for aluminum oxide Al_2O_3 in room temperature, $l \approx 35$ nm. It is not unfeasible to have nanoparticles with diameter significantly smaller than mean free path limit. For example 20 nm [29] and 13 nm [30] particle sizes have been reported for Al_2O_3. However, for small particles with large thermal conductivity and small temperature gradients, there is negligible macroscopic difference between fast diffusion and ballistic phonon transport, since the temperature is effectively constant within the particle and thus the boundary conditions for conduction in liquid will be similar and it would be unlikely that pure ballistic heat conduction in single particle could account to the enhancements seen.

Also, ballistic transport is confined to particles, since the mean free path in liquid is significantly lower than in solids. It is therefore unlikely that any ballistic phonon originating from the particle would persist in the liquid for significant distance. Nevertheless, particles in a nanofluid are packed very closely: the average particle separation for 10 nm diameter particles in 5% solution is only 5 nm [7]. It is also possible that, due to the Brownian motion, the distance between particles is locally small enough for a significant time frame that a phonon originating from one particle would continue to an adjacent particle.

The 5 nm average distance at 5% load is at best an optimistic estimate. Lower loads for 10 nm particles yield roughly 10 and 17 nm distances for 3% and 1% respectively. Moreover, significant heat conduction improvements have been reported for Copper particles with diameters approximately 10 nm and volume fraction as small as 0.03% [25]. Nevertheless, ballistic phonons might enhance clustering effect by allowing small gaps between particles.

While it is within the realm of possibility that the nature of heat conduction in the particles or clusters is purely ballistic, we must also consider typical conditions in the measurement or applications. If we assume that the scale of the system is, say 50 nm, i.e. little above the mean free path of phonons in aluminum oxide, we can consider the difference in heat flow between Fourier's model and ballistic transport. The temperature different within extremes of such system are highly unlikely to be significant. For example, in a water based system we must work with a maximum temperature difference of 100 K over the whole system. This means that the temperature gradient over a distance of the particle or even a cluster is almost nonexistent. Therefore also the difference between diffusion and ballistic transfer is likely not measurable.

Furthermore, if we consider nanoemulsions, i.e. suspensions of liquid droplets, where the mean free path is negligible, we immediately see that ballistic heat transfer cannot have any measurable effect and thus the explaining power of this model is further discredited.

2.4 Liquid layering

It has been observed that liquid near a solid wall exhibits a degree of ordering [31][32] unlike "free" fluid. The interaction between the molecules of the fluid and solid determines the magnitude of the ordered layer: sufficiently strong bonding leads to crystal-like structure in the liquid near the surface. The thermal conduction properties of solids result from their long phonon mean free path and therefore, as the fluid becomes more ordered or "solid-like", the fluid's phonon mean free path also increases and with it the thermal conductivity.

A relatively simple approach would be to consider the increased effective volume fraction [33]. The particle and the surrounding ordered liquid layer, as illustrated in figure 2.2, can then be considered to form a composite entity of radius $r = r_p + d_{layer}$, where r_p is the radius of the particle and $d_{layer} \equiv d_l$ the thickness of the layer. The composite particle has thermal conductivity

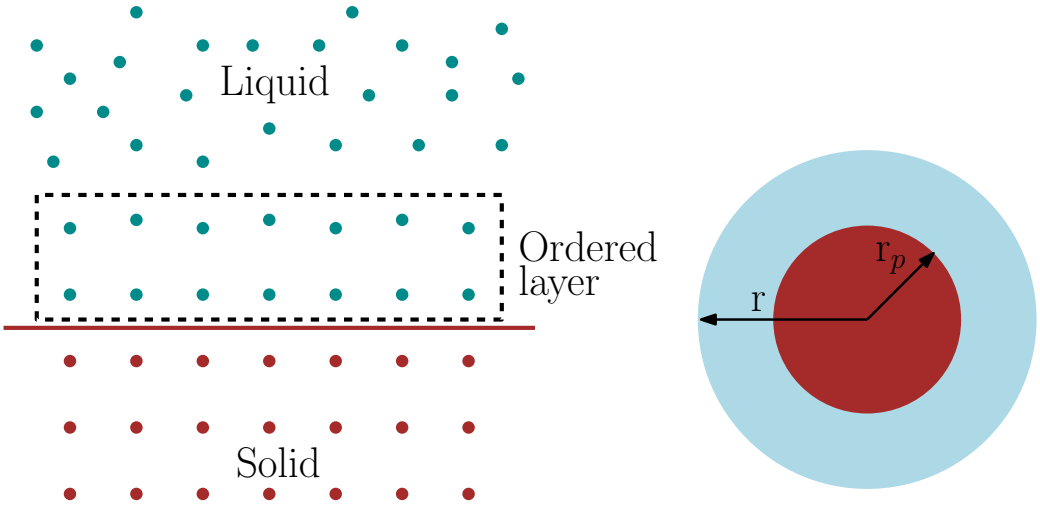

Figure 2.2: Liquid molecules near a solid surface for an ordered layer resembling solid and thus increasing heat conduction. Therefore we consider a composite entity of radius r consisting of a particle with radius r_p surrounded by ordered liquid layer of thickness $d_{layer} = r - r_p$

of k_c and effective volume fraction

$$\phi_c = \frac{\frac{4}{3}\pi(d_l + r_p)^3 n}{V_{tot}} = \frac{\frac{4}{3}\pi r_p^3 n}{V_{tot}}(1 + d_l/r_p) = \phi_p(1+\beta)^3, \tag{2.20}$$

where n is the number of particles, V_{tot} is the volume of the system, ϕ_p the volume fraction of original particles and $\beta = d_l/r_p$. Using the modified volume fraction, Maxwell's formula becomes

$$k_{layering} = \frac{k_c + 2k_f + 2(k_c - k_f)(1-\beta)^3\phi_p}{k_c + 2k_f - (k_c - k_f)(1+\beta)^3\phi_p}k_f, \tag{2.21}$$

where k_c is defined as

$$k_c = \frac{[2(1-\gamma) + (1+\beta)^3(1+2\gamma)]\gamma}{-(1-\gamma) + (1+\beta)^3(1+2\gamma)}k_p, \tag{2.22}$$

where $\gamma = k_{layer}/k_p$ and k_{layer} is the conductivity of the ordered layer. It should be noted that at the limit $d_l + r_p \approx r_p$, $k_{layering} \approx k_{Maxwell}$.

This accounting for liquid layers predicts significant increases in conductivity only to a small subset of nanofluids, namely for very small particles of radii 10nm and less. The conductivity enhancement relative to the Maxwell model is shown in figure 2.3. The conductivity of the layer has minimal effect on the conductivity of the nanofluid whereas the thickness of the layer is mostly responsible for effects on conductivity.

However, a significant portion of the reported increases in thermal conductivity are for particles with radii over 10 nm whereas the liquid layering theory outlined above predicts only minuscule increase for radii larger than 15 nm.

As we are considering the interfacial effects between the fluid and the particle, we must also take into account the Kapitza resistance R_K [34][35] to form a full picture of the composite entity of particle and ordered fluid. R_K exists even at perfect interfaces as it arises from differences in material properties at the interface. Because of these differences, a phonon may scatter from the interface resulting in a decreased flux through it. Flux through the interface is

$$\vec{q} = G\Delta T, \tag{2.23}$$

where $G = 1/R_K$. As a measure of relative importance of the interfacial resistance, so called equivalent thickness of crystal can be defined as

$$h = \frac{k}{G}, \tag{2.24}$$

where k is the thermal conductivity of the fluid. For large particles of diameters 10 μm and up, interfacial resistance has very little effect and it can be comfortably approximated away in most calculations, but the size of particles or droplets in a nanoscale colloids is usually of the order of 10 nanometers, meaning that even a low value of h can have significant effect on the heat conduction across the interface. An estimate of the magnitude of the Kapitza resistance was calculated by Jang et al. to be of the order 10^{-7} cm^{2}K/W [36]. Based on this estimate, the Kapitza resistance can be comfortably neglected as it has no significant effect.

Both simulations and experimental studies of the ordered layer's thickness exist. Molecular dynamic simulations of liquid confined between two walls show that the heat conductivity of a fluid between two walls increases when the distance between the walls is 2 nm, but for wall to wall distance of 27 nm, no conductivity enhancement was found compared to the bulk fluid [37]. Puliti et al. found the liquid layer in the neighborhood of gold nanoparticle in water to extend approximately 0.7 nm from the surface of the particle based on a simulation [38]. However, it should be noted, that the simulation used a relatively small particles of diameters 6.6 nm and less, while most published experimental studies are for larger particles. Nevertheless, another study suggested a value of similar order, namely 0.5 nm [39].

Based on current research and simple modifications to the Maxwell's formula, definitive conclusions are difficult to draw. On one hand, the effect is real and observed, but any effect it has in the case of well dispersed particles

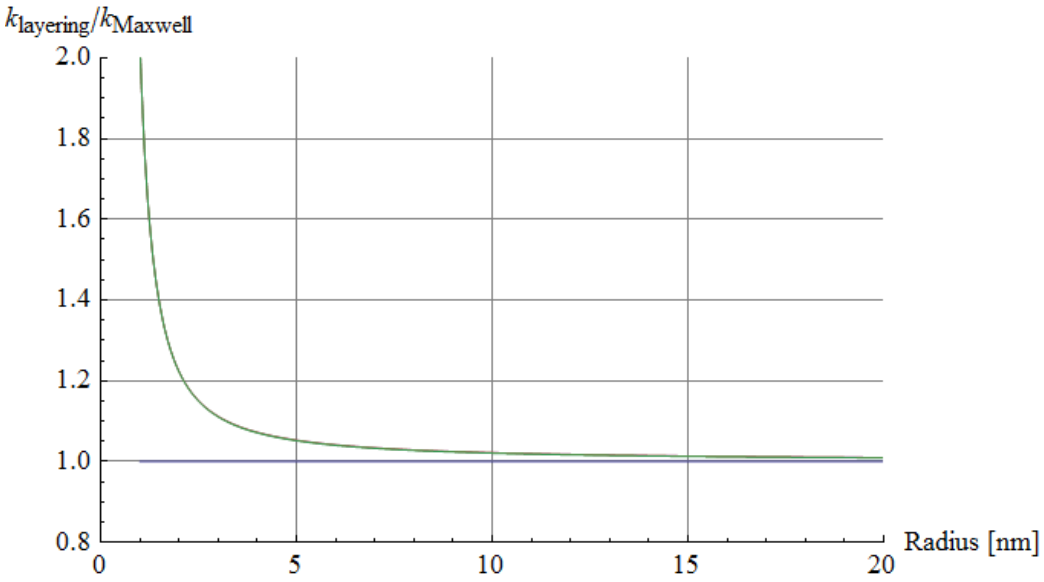

Figure 2.3: The ratio $k_{layering}/k_{Maxwell}$ shows increased conductivity for very small particles. Plot is for 2% volume fraction of copper particles in water with 2 nm thick ordered layer. Values for k_{layer} are 50%, 100% and 1000% of the conductivity of copper, but conductivity of the layer has negligible effect on the conductivity of the nanofluid.

of diameter larger than 20 nm is negligible. However, if the assumption of well dispersed particles is false and particle agglomerates form in the nanofluid, even a thin layer of ordered liquid between particles might enhance the effect of clustering. The clustering of particles is discussed in more detail in the next section.

Comprehensive data on the thermal conduction of nanoemulsions has not yet been published, but the few studies available suggest similar enhancements in liquid-liquid colloids. As the formation is an phenomenon of liquid-solid interface, nanoemulsions would not form such a layer around the droplets. Therefore, liquid layering cannot be responsible for any thermal conductivity enhancements observed in nanoemulsions. However, the expression for the conductivity of a composite particle remains useful while studying a droplet coated by surfactant molecules.

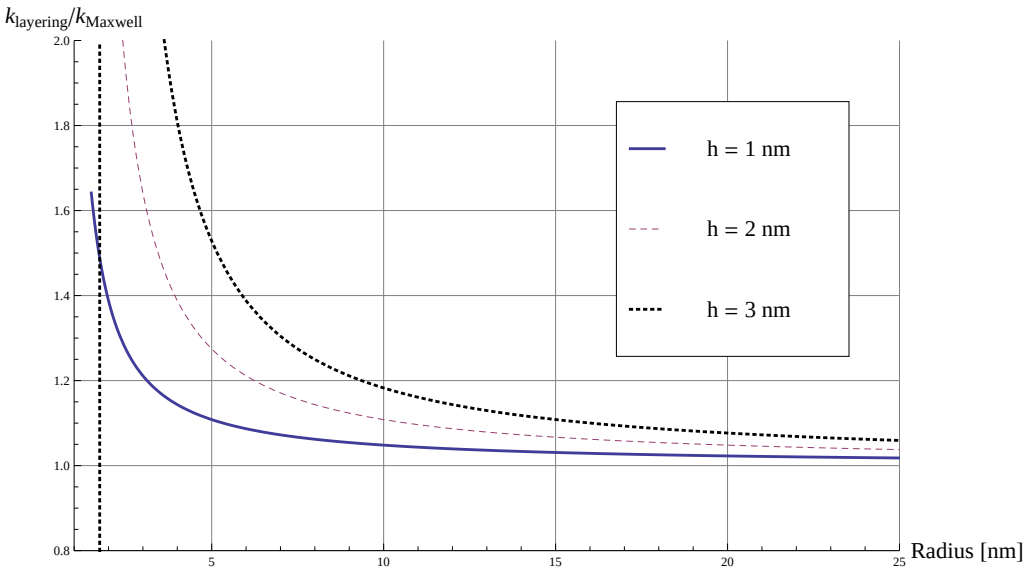

Figure 2.4: The effect of the thickness of the ordered layer. Conductivity enhancement is strongly dependand on the thickness of the layer Volume fraction of copper in water is 2%.

2.5 Particle clustering

Particle clustering can be accounted by two models. First we consider the formation of composite particles. Even the most efficient packings of spherical particles contain empty space, i.e. the packing efficiency of hard spheres is less than one. Since the length scale and the temperature gradient around the particle are both small, we can assume that the composite particle behaves as a single particle of volume $V' = V/\eta_{packing}$, where V is the volume of particles forming the cluster. Therefore the effective volume fraction of the particles increases at lower packing ratios. The hightest efficiency of connecting equal spheres is $\pi/3\sqrt{2} \approx 0.74$ [40] and thus siginificant portion of the agglomerate is filled with the base fluid. The packing efficiency for real particles can naturally be higher than the limit for ideal spheres since the particles are not perfectly uniform in size and shape. As paths of high conductivity can be drawn across the cluster, the whole cluster can be thought as a single particle increasing the effective volume fraction to $\phi' = \phi/\eta$, where η is the efficiency of the packing. Results of this simple modification to Maxwell's model are presented in figure 2.5. However, the simple accounting for the increased effective volume fraction yields only moderate effects on volume

fractions between 1 and 5 %.

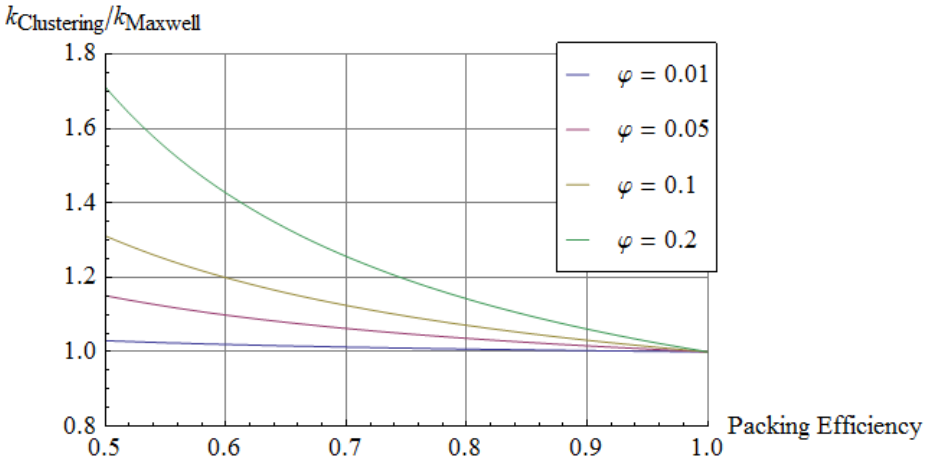

Figure 2.5: The effect of clustering efficiency to the heat conductivity relative to the unmodified Maxwell's model

Second clustering effect improving thermal conduction would be the agglomeration to percolating patterns such that paths of high conductivity are created through the medium. It should also be noted that the orientation of the paths is important to the thermal conductivity of the nanofluid. Upper and lower bound estimates for different orientations of the strands, as illustrated in figure 2.6, can be obtained by modeling the fluid as a thermal circuit. The bounds are thus

$$\frac{q_{series}}{q} = \frac{1}{\left[(1-\phi) + \frac{k_f}{k_p}\phi\right]} \tag{2.25}$$

for a system where the particle agglomerates are oriented in series and flux for a geometry where they are in parallel is

$$\frac{q_{parallel}}{q} = \left[(1-\phi) + \frac{k_p}{k_f}\phi\right], \tag{2.26}$$

where k_f and k_p are the thermal conductivities of the fluid and the particles respectively, ϕ is the volume fraction of the particles and q the value for the base fluid. For parallel orientation, the conduction increases linearly with the volume fraction and the particle thermal conductivity as opposed to series

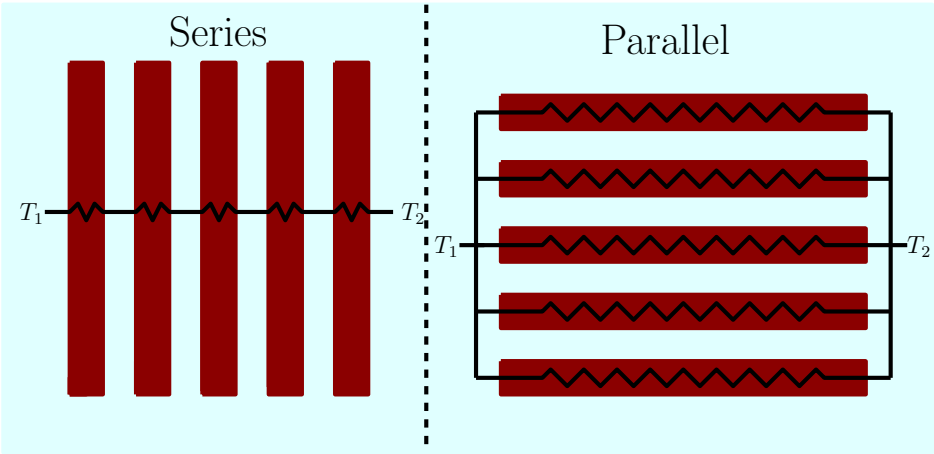

Figure 2.6: The conductivity through "strands" of particles is highly dependand on the orientation of the strands.

conduction where the heat flux with particles is approximately that of the base fluid. For example, $q_{parallel}/q = 6$ for 1 volume % of gold particles in water resulting in significant increase in an ideal system. However, such model is extremely sensitive to discontinuities or disordering of the paths. Thus for a fluid in motion any enhancements from clustering would likely be lost. Also long particle chains require significant particle loading while significant enhancements have been observed at fractions less than 1%.

For example, Kim et al. [41], observed elongated structures, such as in figure 2.7. However, ordinary TEM imaging might change the particle dispersion, since the sample must be dried to obtain an image. A more accurate result could be obtained using a cryo-TEM, where the suspension is frozen nearly instantaneously before imaging and thus the colloid structure is more likely to be preserved.

There have been multiple instances of molecular dynamics simulations supporting the clustering hypothesis [42][43][44][45]. However, several experimental studies have taken the opposite stance observing that thermal conductivity decreases with greater nanoparticle agglomeration [46][47][48] but others have observed local clustering [49][25]. Thus, the effect remains controversial and no conclusive remarks can be made at this point. It still should be noted that significant enhancements have been observed at volume fractions well below the percolation threshold.

Again, nanoemulsions might shed light to the heat conduction enhancement mechanisms. Formation of clusters is highly unlikely if not impossible. When the droplets come into contact, they might merge and thus minimize the surface area, rather than form a cluster or a chain, but this if anything

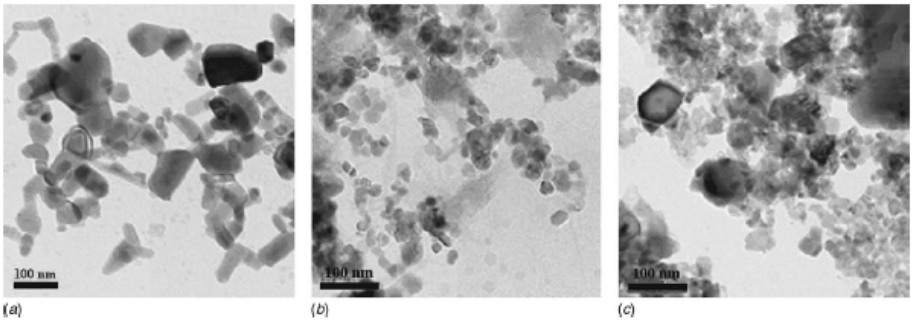

Figure 2.7: TEM images of ZnO nanofluids of three different sizes (a) 60 nm b) 30 nm c) 10 nm). Picture from [41].

hinders the heat conduction and stability. Even if we assume that droplet chains would somehow form, the important factor λ_p/λ_f is of the order of unity for most fluids compared to, for example, the ratio of gold and water, which is 511. However, for other materials commonly used in nanofluids such as silicon dioxide the ratio is approximately 2.3 meaning that equation (2.26) would yield $q_{parallel}/q = 1.013$ for 1% SiO_2 in water.

As we have noted, since neither liquid ordering nor clustering can physically explain the increases observed in heat conduction of nanofluids, some other effect must be chiefly responsible for the increases.

Effect of clustering on viscosity

It should be noted that significantly increased viscosity of a fluid is adverse to its utility in convective application since a more viscous fluid requires more pumping power to achieve similar flow regime than a less viscous medium, meaning that for an application it might be more efficient to use a less viscous liquid whose heat transfer characteristics are worse at higher pumping power than the nominally better nanofluid. We tackle the issue of nanofluid efficiency in chapter 4.

Especially agglomeration into long strands could be adverse to the viscosity of the fluid. Most measurements of the viscosity of the nanofluids report increases higher than the conventional models predict.

2.6 Brownian motion

Brownian motion is a phenomenon where small particles suspended in a stationary fluid move randomly, first observed by Robert Brown in 1827 [50]

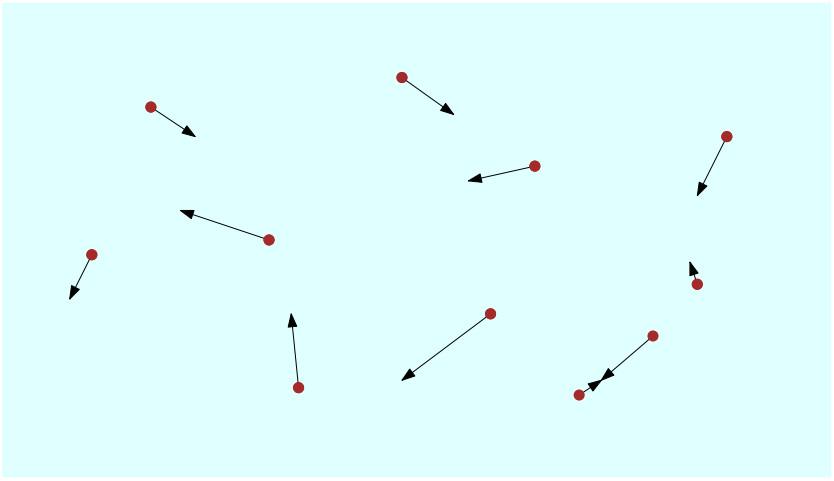

Figure 2.8: Small particles in liquid move randomly. Arrows represent the momenta of particles. The random movement of particles brings about collisions and the particle-particle distance can be very short momentarily

and formally explained by Einstein in 1905 [51].

An important characteristic of the motion of particles in the medium is the diffusion constant

$$D = \frac{k_B T}{6\pi\mu r}, \tag{2.27}$$

where k_B is the Boltzmann constant, T the temperature, μ the viscosity of the medium and r the radius of the particle. From it we notice that the diffusion of the particles is inversely related to the particle size and viscosity and related to the temperature, i.e. the effect of Brownian motion is more pronounced with smaller particles. It is thus feasible that any Brownian effects on the thermal conductivity of nanofluids would not be observable in systems of larger particles.

The diffusion constant can be derived from the Langevin equation relatively straightforwardly. The Langevin equation [52] is

$$m\frac{d^2x}{dt^2} = -\gamma\frac{dx}{dt} + R(t), \tag{2.28}$$

where $R(t)$ is a random force and γ a damping factor. If we multiply both sides by x and take averages, we get

$$m\left\langle x\frac{d^2x}{dt^2}\right\rangle = -\gamma\left\langle x\frac{dx}{dt}\right\rangle + \langle xR(t)\rangle\,. \tag{2.29}$$

The first term is

$$m\left\langle x\frac{d^2x}{dt^2}\right\rangle = m\frac{d}{dt}\left\langle x\frac{dx}{dt}\right\rangle - m\left\langle\left(\frac{dx}{dt}\right)^2\right\rangle, \tag{2.30}$$

where xu_x is independent of time and mu_x^2 is the kinetic energy which on average is k_BT resulting in $m\langle x(d^2x/dt^2)\rangle = k_BT$. The second term is

$$-\gamma\left\langle x\frac{dx}{dt}\right\rangle = -\frac{\gamma}{2}\frac{d\langle x^2\rangle}{dt}. \tag{2.31}$$

By its very definition, the average of the random force is zero. The equation thus becomes

$$-k_BT = -\frac{\gamma}{2}\frac{d\langle x^2\rangle}{dt} \Longleftrightarrow \frac{d\langle x^2\rangle}{dt} = \frac{2k_BT}{\gamma}. \tag{2.32}$$

Einstein relation states $d\langle x^2\rangle/dt = 2D$ and γ is defined by Stokes' relation as

$$\gamma = 6\pi\mu r \tag{2.33}$$

we get the equation for the diffusion coefficient presented at the beginning of the section

$$D = \frac{k_BT}{6\pi\mu r}. \tag{2.34}$$

Particles themselves carry very little thermal energy. An estimation was done by Keblinskin et al. [7], who considered the time it takes for a particle to move a distance equal to its size

$$\tau_D = \frac{d^2}{6D}. \tag{2.35}$$

This quantity is then compared to the time scale for thermal diffusion for the same distance, which is

$$\tau_H = \frac{d^2}{6\alpha}, \tag{2.36}$$

where α is thermal diffusivity defined as $\alpha = k/\rho c_p$. For example, the ratio $\tau_\delta = \tau_D/\tau_H$ for particles of diameter 10 nm in room temperature water is $\tau_\delta = 500$ meaning that the heat transfer via particle movement is 500 times slower than ordinary conduction. Even for particles nearing atomic size of diameter $d \approx 0.5$ nm the ratio is still $\tau_\delta \approx 25$. The simple estimation thus suggests that the effect of thermal energy carried with particles is negligible compared to the thermal diffusion. This conclusion was expected since specific heats of

most particle materials that are used in nanofluids are very small compared to the basefluid.

However, such simple consideration does not take into account the convection of fluid caused by the particle motion. One of the initial considerations taking into account was a model presented by Koo and Kleinstreuer [53], which took into account fluid particles dragged along with the nanoparticles and thermophoretic effects. Another model by Jang and Choi [54] considered a purely Brownian convection and they successfully predicted the temperature and size dependencies. However, their model requires multiple assumptions.

However, according to Prasher et al. [55], the assumptions made by Jang et al. were mostly unphysical. Furthermore, they presented a semi-empirical model taking into account convective effects [56]. They argued that convection is felt almost instantly at distance equal to the particle distance meaning that timescale $\tau_{convection} \ll \tau_D$. The argument for this model is based on consideration of a sphere inbedded in a semi-infinite medium. The Reynolds number for 10 nm diameter Al_2O_3 particles is 0.029 and thus in the Stokes regime. In such situation from the first principles it can be shown that the heat transfer coefficient is $h = (k_f/r_p)[1 + (1/4)\mathrm{Re} \times \mathrm{Pr}]$. The conductivity for nanofluids is thus

$$\frac{k}{k_f} = \left(1 + \frac{Re_B \times Pr}{4}\right)\left(\frac{[k_p(1+2\alpha)+2k_f] + 2\phi[k_p(1-\alpha)-k_m]}{[k_p(1+2\alpha)+2k_f] - \phi[k_p(1-\alpha)-k_f]}\right), \quad (2.37)$$

where Re_B is the so-called Brownian Reynolds number

$$Re_B = \frac{1}{\nu}\sqrt{\frac{18k_BT}{\pi\rho d}}, \quad (2.38)$$

where ν is the kinematic viscosity. k_f is the conductivity of the medium and $\chi = 2R_bk_f/d$, where R_b is the interfacial resistance between the particle and fluid. The model, when fitted to empirical data provides a relatively good agreement with different data sets from experiments. A more recent study [57] however indicates that the actual heat flux due to the kinetic contribution is negligible and that the increases are caused by the interaction between the particles.

The status of Brownian motion, as with other propositions, is still contested with arguments both against and for it. However, the Brownian motion model has certain elegance to it. It is agnostic to the properties of the particles and thus it is the only proposition capable of explaining the observed increases for nanoscale emulsions. Furthermore, no assumptions have to be made about the thickness or properties of the ordered layer or

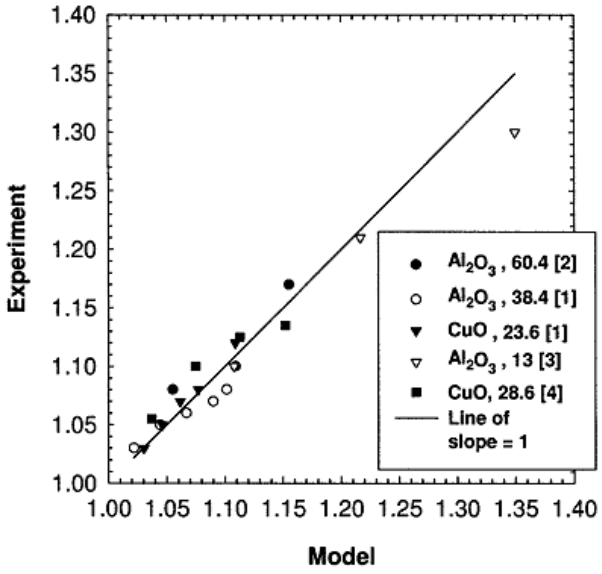

Figure 2.9: Comparison of a semi-experimental model by Prasher et al. [55]. The model generally predicts very similar values as the measurements.

the orientation or formation of the agglomerates. However, exact theoretical formulation is very difficult without a large number of parameters.

Chapter 3

Convective heat transfer

The second chapter considered only thermal conduction of matter whereas most heat transfer applications are specifically implementations of thermal convection i.e. heat transfer caused by movement of bulk matter. Furthermore, for most studies, only stationary fluid was considered. Clearly, this picture is incomplete especially from the point of view of applications.

Convection is more complex phenomenon than thermal conduction. Laminar flow is well understood and exact solutions can be presented for many geometries but the turbulent flow is not as well understood. It is still unknown if an analytic solution exists or not. In this chapter we will discuss the classical theory for bulk matter and review models taking into account microscopic phenomena.

In this section, we generally follow the approach and notation of Bergman et al. [58] while discussing the laminar flow and empirical correlations.

3.1 Dimensionless numbers

The examination of conduction utilizes a few dimensionless numbers that characterize the heat transfer and the flow of the fluid. The three most important dimensionless numbers are the Nusselt, the Prandtl and the Reynolds number.

3.1.1 Nusselt number

The Nusselt number, which can be thought as a dimensionless heat transfer coefficient, is defined as

$$\mathrm{Nu} = \frac{hL_c}{k}, \tag{3.1}$$

where k is the thermal conductivity of the fluid, L_c the characteristic length of the system and h the heat transfer coefficient. As can be readily observed, the Nusselt number relates conduction to convective heat transfer such that larger Nusselt numbers signify greater fraction of the heat transfer is convective. It should be noted that for the average Nusselt number the following holds

$$\langle \mathrm{Nu} \rangle = f(Re, Pr), \tag{3.2}$$

where Re is the Reynolds number and Pr the Prandtl number and f is an arbitrary function.

3.1.2 Prandtl number

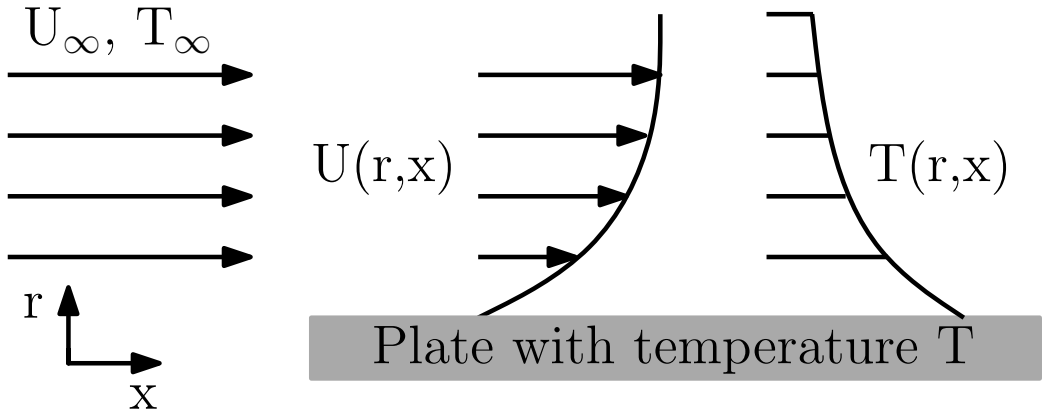

Figure 3.1: A fluid has a free stream velocity u_∞ and temperature T_∞ before meeting a heated plate with temperature T such that $T > T_\infty$. Interaction with the plate slows the velocity of the fluid and thus forms a velocity gradient. Similarly, a temperature gradient is formed.

Consider a fluid flowing on top of a heated plate. Before the plate, the fluid has velocity u_0 and temperature T_0. We define hydrodynamic boundary layer as the region of the flow where viscous forces are felt i.e. where the contact with the plate slows the velocity of the fluid to $u_f < u_0$. Similarly, the thermal boundary layer is defined as the region of the flow where temperature gradients exist.

In such context, the Pradtl number provides a relation between the momentum and energy transport by diffusion in the velocity and thermal boundary layers. It is defined as

$$\mathrm{Pr} = \frac{v}{\alpha} = \frac{\mu c_p}{k}, \tag{3.3}$$

where nu is the kinematic viscosity, $\alpha = k/(\rho c_p)$ the thermal diffusivity, c_p is the specific heat, μ the dynamic viscosity and k the thermal conductivity.

3.1.3 Reynolds number

The Reynolds number is a dimensionless quantity that describes the ration of the inertial forces to viscous forces. It is used to characterize the flow of the fluid, i.e. is it laminar, in transition regime or turbulent. At small Reynolds numbers, viscous forces outweigth the inertial forces and keep the flow "ordered", that is, the flow is laminar. It is defined as

$$\mathrm{Re} = \frac{\rho V L_c}{\nu}, \tag{3.4}$$

where ν is the kinematic viscosity, V the velocity of the fluid and ρ is the density of the fluid. In pipe flow, the characteristic length is the hydraulic diameter of the pipe which for a round tube is simply the diameter of the tube.

3.1.4 The continuum hypothesis and Knudsen number

All discussion in this section assumes that the continuum hypothesis holds, i.e. that the fluid is treated as a continuous medium. The length scales of a system are related through the Knudsen number

$$\mathrm{Kn} = \frac{\lambda}{l}, \tag{3.5}$$

where λ is the mean free path of the fluid molecules and l is the characteristic length of the system. Generally, the continuum hypothesis is valid if Kn$\ll$ 1. In most flow systems the shortest relevant distance is of the order of millimeters and the mean free paths are of the order of nanometers and thus the fluid can be treated as a continuous medium in most applications.

3.2 Laminar tube flow

In this section we will consider the fully developed laminar flow of incompressible Newtonian fluid with constant properties in a circular tube. In the fully developed region the radial velocity component and the gradient of the axial velocity are zero

$$v_{radial} = 0, \text{ and } \frac{\partial u(x,r)}{\partial x} = 0, \tag{3.6}$$

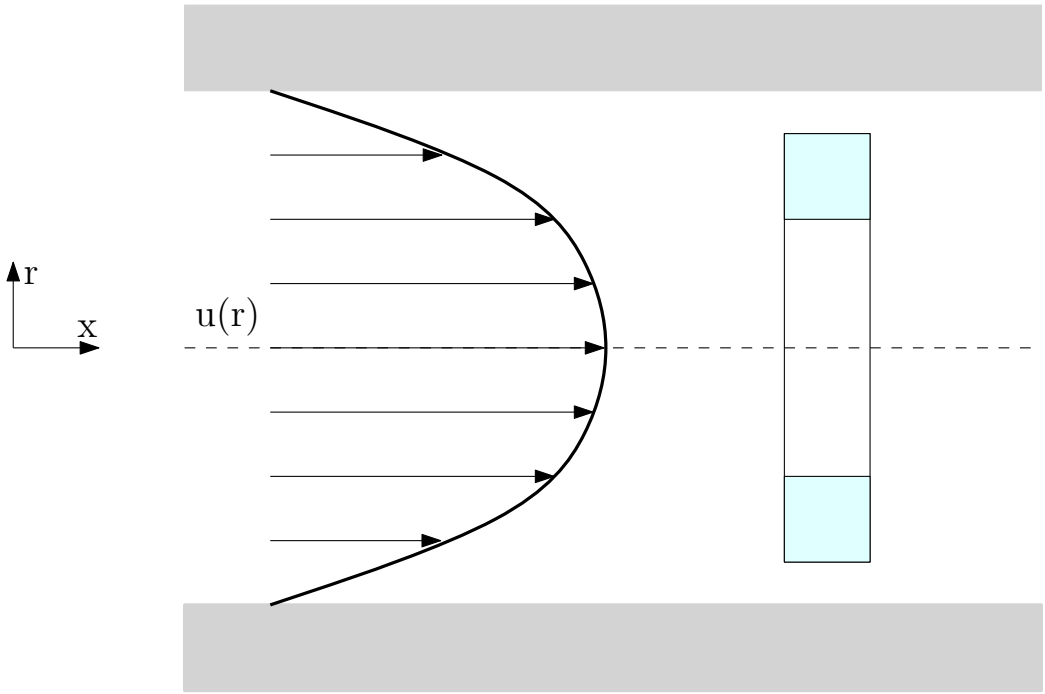

Figure 3.2: The velocity profile of a fully developed flow in a circular pipe. To derive the velocity profile, we consider the force balance of an annular differential element shown in light blue.

and thus $u(x, r) = u(r)$. The velocity may be obtained from the appropriate momentum equation. Consider an annular differential element as illustrated in figure 3.2. The force balance is

$$\tau_r(2\pi r dx) - \left\{\tau_r(2\pi r dx) + \frac{d}{dr}\left[\tau_r(2\pi r dx)\right] dx\right\} + p(2\pi r dx) - \left\{p(2\pi r dx) + \frac{d}{dx}\left[p(2\pi r dr)\right] dx\right\} = 0. \quad (3.7)$$

Expanding this, we find that it reduces to

$$-\frac{d}{dr}(r\tau_r) = r\frac{dp}{dx}. \quad (3.8)$$

The stress becomes

$$\tau_r = -\mu\frac{du}{dr}. \quad (3.9)$$

Using it, we obtain the following differential equation for the velocity profile

$$\frac{\mu}{r}\frac{d}{dr}\left(r\frac{du}{dr}\right) = \frac{dp}{dx}. \quad (3.10)$$

Since the pressure gradient is independent of r, the equation may be solved by integrating twice with regard to r which yields

$$u(r) = \frac{1}{\mu}\left(\frac{dp}{dx}\right)\frac{r^2}{4} + C_1 \ln(r) + C_2. \tag{3.11}$$

The constants can be determined by using two boundary conditions, namely that the velocity at the surface is zero, i.e. $u(r_0) = 0$ and that there is radial symmetry at the centerline $(\partial u/\partial r)_{r=0} = 0$. Thus we obtain

$$U(r) = -\frac{1}{4\mu}\left(\frac{dp}{dx}\right) r_0^2 \left[1 - \left(\frac{r}{r_0}\right)^2\right]. \tag{3.12}$$

The pressure gradient can be determined using the mean velocity of the fluid

$$u_m = \frac{2}{r_0^2}\int_0^{r_0} u(r,x) r dr. \tag{3.13}$$

Mean velocity can be easily obtained from the knowledge of mass flow and the geometry of the system. Thus the velocity profile is

$$\frac{u(r)}{u_m} = 2\left[1 - \left(\frac{r}{r_0}\right)^2\right]. \tag{3.14}$$

Our main focus is on the heat transfer of the tube flow. Thus, we continue considering a fluid that enters a heated tube such that its temperature $T(0,r)$ is uniform and less than the temperature of the surface of the tube. If the temperature T_t or the heat flux q_t is uniform, then, at some point, the temperature profile reaches the fully developed region.

We start by considering the mean temperature over a cross section

$$T_m = \frac{\int_A \rho u c_p T dA_c}{\dot{m} c_p} = \frac{2}{u_m r_0^2}\int_0^{r_0} uTr dr. \tag{3.15}$$

The mean temperature can be used to obtain the advected thermal energy by multiplying equation (3.15) by $\dot{m}c_p$.

In contrast to the fully developed velocity profile, where velocity profile did not change with longitudinal coordinate x, $dT_m/dx \neq 0$ if there is heat transfer. Therefore, the temperature profile changes continuously and thus does not have similarly defined fully developed region as the fluid flow. However, we can introduce a dimensionless temperature difference

$$\xi = \frac{T_s(x) - T(r,x)}{T_s(x) - T_m(x)}. \tag{3.16}$$

This is interpreted such that the relative shape of the profile does not change in the thermally fully developed region and the condition is

$$\frac{\partial \xi}{\partial x} = 0. \tag{3.17}$$

This condition is eventually reached if the aforementioned condition, i.e. uniform temperature or heat flux is in effect. It should be noted that both conditions cannot be simultaneously achieved. An example of a uniform temperature would be a system whose temperature is set by a phase change, i.e. condensing or boiling happening at the outer surface.

Continuing with equation (3.17) and evaluating at $r = r_0$, we find

$$\frac{-\frac{\partial T}{\partial r}|_{r=r_0}}{T_s - T_m}, \tag{3.18}$$

which does not depend on x. Utilizing the Fourier's law

$$q_s'' = k\frac{\partial T}{\partial r}|_{r=r_0}, \tag{3.19}$$

and the Newton's law of cooling

$$q_s'' = h(T_s - T_m), \tag{3.20}$$

we immediately see that

$$\frac{h}{k} \neq f(x), \tag{3.21}$$

i.e. in thermally fully developed flow the local convection coefficient is constant.

3.3 Turbulent flow

As seen before, the laminar tube flow is a phenomenon that can be treated analytically. However, turbulent flow is characterized by chaotic property changes such as variation in pressure and velocity in space and time, and the exact mathematical formulation - or proof that it is not possible - is one of the greatest unsolved problems in mathematics[1]. Therefore an in depth

[1]The difficulty of turbulence is perhaps illustrated best by an amusing anecdote: Horace Lamb, an applied mathematician who studied fluid flow, is reported to have said at the meeting of the British Association in 1932 "I am an old man now, and when I die and go to Heaven there are two matters on which I hope for enlightenment. One is quantum electrodynamics and the other is the turbulent motion of fluids. And about the former I am really rather optimistic." [59]

discussion of turbulent phenomena is well beyond the scope of this thesis. However, we will perform a concise overview of the turbulent phenomena in the form of Reynolds mean flow equation and empirical correlations. In this section, we follow the approach of the book by S. Pope [60] unless otherwise noted.

3.3.1 Mean flow equation

In turbulent flow, the velocity of the fluid $u(x,t)$ is a random variable. However, the velocity is a solution to a completely deterministic equation. Therefore, the velocity is fully determined from the initial conditions of the equation of motion. However, in experiments, the initial conditions can never be fully controlled and very small perturbations can cause large fluctuations in the solution. An example of such chaotic behavior would be the following system of differential equations, known as the Lorenz equations,

$$\begin{aligned} \dot{x} &= \sigma(y-x), \\ \dot{y} &= \rho x - y - xz, \\ \dot{z} &= -\beta z + xy, \end{aligned} \tag{3.22}$$

where x, y, z are functions of time and $\dot{x}$ refers to derivative with respect to t. The difference of solutions with different initial conditions $x(t) - x'(t)$ is shown in figure 3.3. The initial conditions are $[x(0) = y(0) = z(0) = 0.1]$ and $[x(0) = 0.100001, y(0) = z(0) = 0.1]$.

Since the small perturbation that could cause the fluctuations in turbulent are also present in the laminar situation, their mere presence cannot explain the randomness of turbulent flow. The Navier-Stokes equation applies equally in the turbulent regime, but to obtain useful information, exact solutions cannot be considered.

One approach is to consider the Reynolds decomposition

$$u(x,t) = \langle u(x,t) \rangle + u^*(x,t), \tag{3.23}$$

where the velocity is separated to its mean and the fluctuation u^*. From the continuity equation we see that

$$\nabla \cdot (\langle u(x,t) \rangle + u^*(x,t)) = 0. \tag{3.24}$$

For the following discussion, we define the material derivative

$$\frac{D}{Dt} = \frac{\partial}{\partial t} + u_i \frac{\partial}{\partial x_i} \tag{3.25}$$

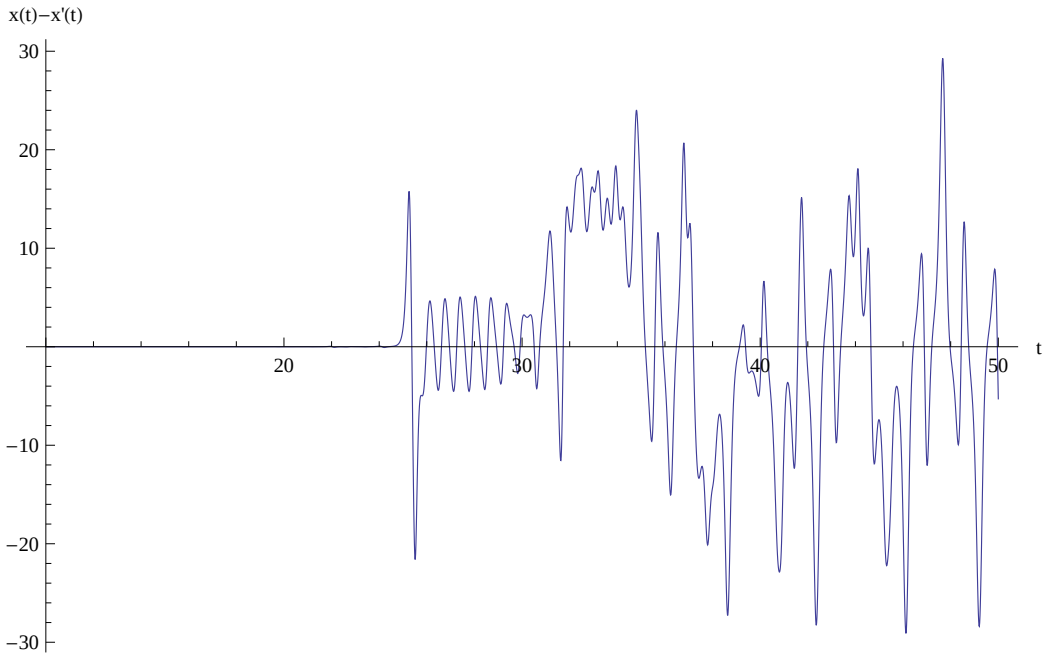

Figure 3.3: Difference of two solutions to equations (3.22) using two sets of initial conditions.

We want to take the mean of the momentum equation

$$\frac{Du}{Dt} = -\frac{1}{\rho}\nabla p + \nu\nabla^2 u, \tag{3.26}$$

where p is the pressure, but it is not as straightforward as with the continuity equation. First, consider the material derivative in conservative form

$$\frac{Du_j}{Dt} = \frac{\partial u_j}{\partial t} + \frac{\partial(u_i u_j)}{\partial x_i}, \tag{3.27}$$

and take the mean

$$\left\langle \frac{Du_j}{Dt} \right\rangle = \frac{\partial\langle u_j\rangle}{\partial t} + \frac{\partial\langle u_i u_j\rangle}{\partial x_i}. \tag{3.28}$$

Using Reynolds decomposition, we can write the $\langle u_j u_i\rangle$ term as

$$\begin{aligned}\langle u_j u_i\rangle) &= \langle(\langle u_i\rangle u_i^*)(\langle u_j\rangle + u_j^*)\rangle \\ &= \langle\langle u_i\rangle\langle u_j\rangle + u_i^*\langle u_j\rangle + u_j^*\langle u_i\rangle + u_i^* u_j^*\rangle \\ &= \langle u_i\rangle\langle u_j\rangle + \langle u_i^* u_j^*\rangle, \end{aligned} \tag{3.29}$$

where we have used the fact that $\rangle u_i^*\rangle = 0$. The mean of the material derivative is thus

$$\left\langle \frac{Du_j}{Dt} \right\rangle = \frac{\partial\langle u_j\rangle}{\partial t} + \langle u_i\rangle\frac{\partial\langle u_j\rangle}{\partial x_i} + \frac{\partial}{\partial x_i}\langle u_i^* u_j^*\rangle, \tag{3.30}$$

where a term containing the velocity covariances, which are called Reynolds stresses, has appeared. Defining the mean material derivative

$$\frac{\bar{D}}{\bar{D}t} \equiv \frac{\partial}{\partial t} + \langle u \rangle \cdot \nabla, \tag{3.31}$$

we can write the mean-momentum or Reynolds equation

$$\frac{\bar{D}u_j}{\bar{D}t} = \nu \nabla^2 \langle u_j \rangle - \frac{1}{\rho} \frac{\partial \langle p \rangle}{\partial x_j} - \frac{\partial \langle u_i^* u_j^* \rangle}{\partial x_i}. \tag{3.32}$$

The equation is similar to the Navier-Stokes equation, except that the Reynolds equation has a term containing the Reynolds stresses. They can be seen arising from the fluctuating velocity at the boundary of a volume V. A feature of the Reynolds approach is that the system of equations has more unknowns than equations in the form of the Reynolds stresses and thus the equations cannot be solved unless the stresses are determined.

Further discussion of properties turbulence would quickly be counterproductive to the goal of this thesis but the above discussion has shown one type of an approach to the problem of turbulence. Therefore, we shall next present a few well known correlations for pipe flow.

3.3.2 Empirical correlation equations for pipe flow

A traditional correlation equation for heat transfer in a fully developed turbulent flow in a smooth circular tube is the Dittus-Boelter correlation

$$\mathrm{Nu} = 0.023 \ \mathrm{Re}^{0.8}\mathrm{Pr}^{n}, \tag{3.33}$$

where n has the value 0.4 for heating the fluid and 0.3 for cooling. The correlation has been experimentally verified in the range $0.6 \leq Pr \leq 160$, $Re \geq 10^4$ and the ratio of length to diameter $L/D \geq 10$. Furthermore, the correlation is accurate for only moderate temperature differences.

Another correlation that is suitable for larger property variations is the Sieder-Tate formula

$$\mathrm{Nu} = 0.0027 \mathrm{Re}^{\frac{4}{5}} \mathrm{Pr}^{\frac{1}{3}} \left(\frac{\mu}{\mu_s} \right)^{0.14}. \tag{3.34}$$

This equation is valid for Prandlt numbers between 0.7 and 16700. However, both of these equations are somewhat inaccurate and errors may be as large as 25%.

A more accurate correlation is the Gnielinski correlation that is valid for smooth tubes and in the transition region, i.e. for Reynolds numbers from 3000 to $5 \cdot 10^6$. The correlation is

$$\mathrm{Nu} = \frac{(f/8)(\mathrm{Re} - 1000)\mathrm{Pr}}{1 + 12.7(f/8)^{\frac{1}{2}}(\mathrm{Pr}^{\frac{1}{2}} - 1)}, \tag{3.35}$$

where f is the friction factor that can be obtained from the Moody chart.

3.4 A Convective model for nanofluids

Different microphysical effects have been widely considered in the search for an explanation for the increased heat conductivity. However, similar increases in Nusselt number have been achieved in convective investigations. For example, both Xuan and Li [61] and Pak and Cho [62] reported increased Nusselt number relative to a well known Dittues-Boelter correlation while using the nanofluid bulk properties.

Conventional models, taking into account only the bulk properties can be classified as homogeneous models. This approach assumes that the increase in convective heat transfer results only from the thermal and fluid properties of the nanofluid. However, predictions of homogeneous models fail to properly predict increased heat transfer coefficient [63].

We will discuss a model by Buongiorno [64], that takes into account microphysical phenomena via consideration of nanoparticle-base-fluid relative velocity.

3.4.1 Nanoparticle slip

It is possible for a nanoparticle to have a velocity relative to the base fluid called slip velocity. The effects that generate the slip velocity are numerous. Examples include Brownian motion, thermophoresis, diffusiophoresis, Magnus effect and gravity. However, an order of magnitude analysis shows that other effects are negligible compared to the Brownian motion and thermophoresis. Furthermore, in turbulent flow, slip mechanisms become negligible and particles move with turbulent eddies. Therefore particle slip may be important near the wall in the laminar sublayer where the turbulent effects are not important.

The next step is to incorporate the important slip generating effects into the nanofluid transport model. First we consider the nanoparticle and thermophoretic fluxes. Assuming that the nanoparticles are in thermal equilibrium with the surrounding fluid, i.e. have the same average kinetic energy

$\frac{1}{2}k_BT$, the Brownian diffusion coefficient for molecules is the well known Einstein-Stoke's equation

$$D_B = \frac{k_BT}{3\pi\mu d_p}, \tag{3.36}$$

where k_B is the Boltzmann constant, T the temperature of the fluid, μ the viscosity of the fluid and d_p the diameter. The particle mass flux can be expressed as

$$\vec{j}_{p,B} = -\rho_p D_B \nabla\phi, \tag{3.37}$$

where ϕ is the nanoparticle volumetric fraction and ρ_p the density of the particles.

Thermophoresis is a phenomenon, where a temperature gradient causes particles to diffuse. Thermophoretic velocity of the particles is

$$V_T = -\beta\frac{\mu}{\rho}\frac{\nabla T}{T}, \tag{3.38}$$

where

$$\beta = 0.26\frac{k}{2k + k_p}, \tag{3.39}$$

where k is the thermal conductivity of the continuous medium, k_p the thermal conductivity of the particle, μ the viscosity of the medium and ρ the density of the medium and T the temperature. The mass flux due to thermophoresis is then

$$\vec{j}_{p,t} = \rho_p\phi V_T = -\rho_p D_T\frac{\nabla T}{T}, \tag{3.40}$$

where we have defined the thermal diffusion coefficient $D_T = \beta\mu\phi/\rho$

We begin with the continuity equation for the nanofluid

$$\nabla \cdot u = 0, \tag{3.41}$$

where u is the nanofluid velocity. Note that the equation is identical to that of incompressible fluid. The second continuation equation is for the nanoparticles

$$\frac{\partial\phi}{\partial t} + u \cdot \nabla\phi = -\frac{1}{\rho_p}\nabla \cdot \vec{j}_p, \tag{3.42}$$

where $\vec{j}_p$ is the diffusion mass flux of the nanoparticles which is the nanoparticle flux relative to the nanofluid velocity u. If there are no significant external forces, the flux is simply the sum of the Brownian and thermophoretic fluxes

$$\vec{j}_p = \vec{j}_{p,B} + \vec{j}_{p,T}. \tag{3.43}$$

Substituting the above expression into the continuity equation (3.42), it becomes

$$\frac{\partial \phi}{\partial t} + \vec{v} \cdot \nabla \phi = \nabla \cdot \left[D_B \nabla \phi + D_T \frac{\nabla T}{T} \right] \tag{3.44}$$

The right hand side contains the terms that describe the nanoparticle slip velocity due to Brownian motion and thermophoresis. The momentum equation for nanoparticles is

$$\rho \left[\frac{\partial u}{\partial t} + u \cdot \nabla u \right] = -\nabla P - \nabla \cdot \tau, \tag{3.45}$$

where P is the pressure and τ the stress tensor. For a Newtonian fluid, the stress tensor can be expanded as

$$\tau = -\mu [\nabla u + (\nabla u)^T], \tag{3.46}$$

assuming Newtonian behavior and incompressible fluid. The ^{T} indicates the transpose of the vector. If μ is constant, then the momentum equation reduces to the standard Naviers-Stokes equation. However, as we consider a particle suspension, the viscosity of a nanofluid depends on the particle concentration which may vary greatly within the fluid.

The energy equation for nanofluids is

$$\rho c_p \left[\frac{\partial T}{\partial t} + u \cdot \nabla T \right] = -\nabla \cdot \vec{q} + h_p \nabla \cdot \vec{j_p}, \tag{3.47}$$

where $c_{p,f}$ is the nanofluid specific heat, h_p the specific enthalpy of the particle material. Assuming there is no radiative heat transfer, the heat flux can be calculated as

$$\vec{q} = -k \nabla T + h_p \vec{j_p}, \tag{3.48}$$

which is substituted into equation (3.47) resulting in

$$\rho c_{p,f} \left[\frac{\partial T}{\partial t} + u \cdot \nabla T \right] = \nabla \cdot k \nabla T - c_p \vec{j_p} \cdot \nabla T, \tag{3.49}$$

where we have used $\nabla \cdot (h_p \vec{j_p}) = h_p \nabla \cdot \vec{j_p} + \vec{j_p} \cdot \nabla h_p$ and where $\nabla h_p = c_{p,p} \nabla T$, where $c_{p,p}$ is the nanoparticle specific heat and which follows from assuming that the nanoparticles and the fluid are in thermal equilibrium.

The final form of the equation is achieved by substituting the formula for $\vec{j_p}$ in the above equation and thus we have

$$\rho c_{p,f} \left[\frac{\partial T}{\partial t} + u \cdot \nabla T \right] = \nabla \cdot k \nabla T + \rho_p c_{p,p} \left[D_B \nabla \phi \cdot \nabla T + D_T \frac{\nabla T \cdot \nabla T}{T} \right]. \tag{3.50}$$

Consider equation (3.50). It has terms describing heat transport by convection, conduction and nanoparticle diffusion. It should be noted that $\rho c_{p,f}$ is the heat capacity of the whole fluid incorporating heat transfer by nanoparticles moving with the flow.

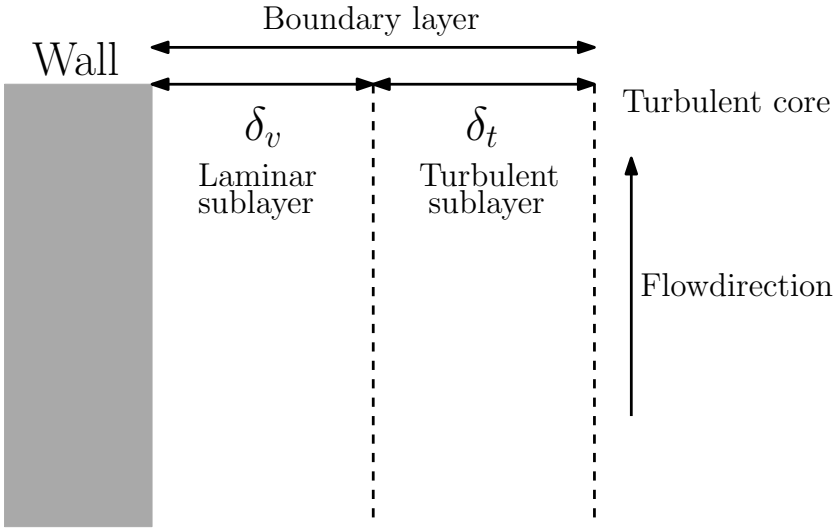

Figure 3.4: Structure of the flow.

The discussion above has led to four equations completely describing the energy-momentum state of the nanofluid. Furthermore, a correlation equation linking Nusselt and Reynolds numbers can be derived.

However, order of magnitude analysis suggests that the heat transfer caused by nanoparticle movement is negligible compared to conventional convection and conduction and thus the particles would affect the heat transfer only through their thermal properties.

Turbulent flow near a wall can be divided into three regions, as in figure 3.4, laminar sublayer δ_v, turbulent sublayer δ_t and the turbulent core. In the laminar sublayer the diffusion constant for Brownian motion is much larger than the eddy particle diffusivity and the viscosity is much larger than the eddy diffusivity of momentum. In the turbulent sublayer, the relations are inverted, i.e. particle diffusion constant is much smaller than the eddy diffusivity. Thus, due to thermophoresis, the nanoparticle fraction near the wall in the laminar sublayer, where particles have significant velocities relative to the fluid, can be lower than in the bulk fluid and thus the viscosity is lowered in the laminar sublayer. Thus Buongiorno [64] arrives at the correlation

$$Nu = \frac{\frac{f}{8}(Re_b - 1000)Pr_b}{1 + \delta_\nu^+ \sqrt{\frac{f}{8}}(Pr_\nu^{2/3} - 1)}, \tag{3.51}$$

where subscript b refers to bulk properties and ν and δ_ν^+ is the dimensionless thickness of the laminar sublayer which is related to the actual thickness as $\delta_\nu \sim \delta_\nu^+ \mu_\nu / \sqrt{\rho\tau}$. However, δ_ν^+ must be determine empirically.

Comparisons with two experimental data sets of aluminum and titanium nanoparticles show very good agreement with experimental data. The advantages of the model are that it includes microphysical phenomena of thermophoresis and Brownian motion and it includes only one empirical coefficient. For example, a dispersion model proposed by Xuan and Li requires five empirical constant to fit the data. Additionally, the limit of $\phi = 0$ reduces to the a pure fluid correlation, namely the Prandtl correlation. The comparison is illustrated in figure 3.5.

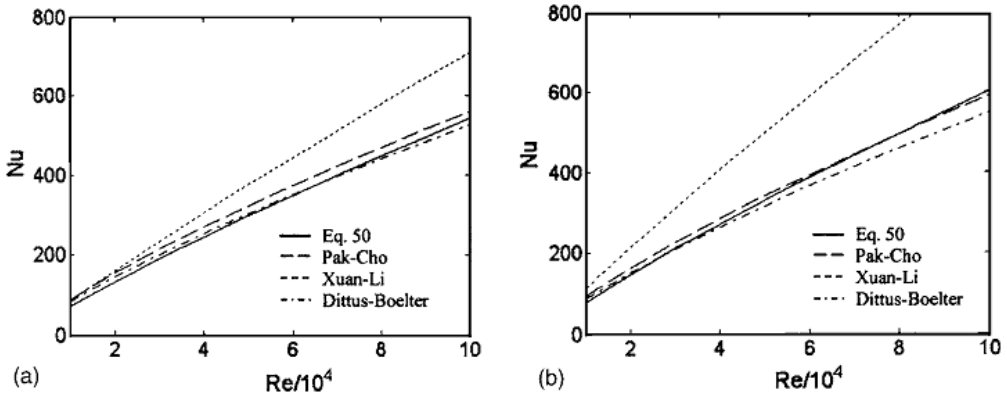

Figure 3.5: Comparison of correlation (3.51) to experimental data and Dittus-Boelter correlation for titanium nanoparticles in water. Particle fractions are 0.01 for a) and 0.03 for b). Figure from [64].

Chapter 4

Experimental methods

In this chapter, we give an overview of the experimental methods utilized in the sample fabrication, characterization and heat transfer measurement.

4.1 Emulsion Fabrication

The experimental focus of this thesis is on n-decane in water emulsions. Generally, an emulsion is a colloid consisting of two immiscible Popularity liquids such that one liquid is dispersed in the other. Emulsions do not form spontaneously but require external energy input. This is doubly true for nanoscale emulsions since breaking of droplets to even smaller ones requires larger energy inputs than formation of microscale emulsions.

The chosen fabrication process is simple: constituents of the emulsion, i.e. continuous and dispersed liquid and a suitable surfactant, are mixed in a suitable container. The mixture is then subjected to ultrasound mixing until sufficient structure is achieved. Ultrasound mixing was chosen because of the simplicity of the procedure and available equipment. Multiple other options for nanoemulsion preparation exist and have been demonstrated [65][66][67]. These include a phase-inversion-temperature method where mixture is heated above a phase inversion temperature and then cooled rapidly. In such process the dispersed phase catastrophically becomes the continuous phase and an emulsion of a small scale is formed. Yet another option is to force the mixture through microchannels which causes significant shear that breaks droplets to smaller ones. Mechanical shear is usually not intensive enough to generate nanoscale emulsions. Nanoscale emulsions also differ from microscale emulsions in that they are very stable once formed.

The factors having an effect on the size and stability of the emulsion are, however, numerous. Examples include but are not limited to choice of sur-

factants, mixing temperature, sample size, mixing power and relative ratios of continuous and dispersed phase and amount and type of surfactants used. Thus, optimization of nanoemulsions is a highly nontrivial problem compared to the preparation of solid particle suspensions where simple sonication is often sufficient.

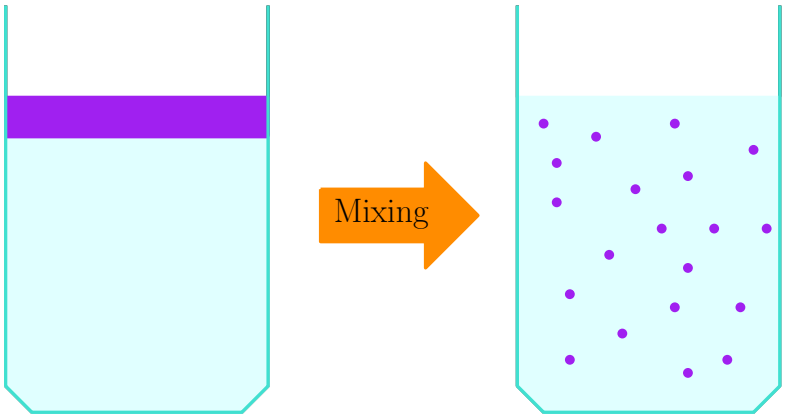

Figure 4.1: Emulsification is a process of forming a metastable colloid from two immiscible liquids. Surfactants are usually added to the mixture to improve stability of the emulsion.

4.1.1 HLB-value

Hydrophilic-lipophlilic balance (HLB) is a number that describes the degree to which a surfactant or a combination of surfactants is hydrophilic or lipophilic. A value of 0 indicates a completely lipophilic molecule.´

4.1.2 Micelles

Micelles, as illustarated in figure 4.2, are a class of self-assembling colloids consisting of aggregates of surfactant molecules dispersed in a liquid. Formation of micelles can be adverse to nanoemulsion formation by lowering the amount of surfactant available for droplet formation and thus changing the droplet size distribution profile and cause false conclusions to be drawn from the size data. In the worst case, if most of the surfactants form micelles, the desired emulsion might not actually be formed at all since sufficient amount of surfactants are not available.

We also consider the possibility of forming pure micelle nanofluids. Such colloid is very easy to manufacture even in large quantities as the formation of micelles is spontaneous and thus requires only the combination of the

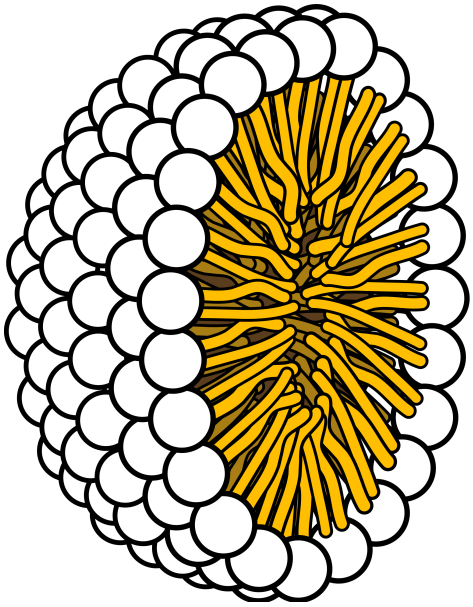

Figure 4.2: A micelle is an aggregate of surfactant molecules.

surfactant molecules and the continuous phase and very gentle stirring. Additionally, the size and shape of the micelles formed can be controlled simply by using different surfactants and as surfactants are a commonly and widely used chemical compound, there exists a myriad of different options to choose from. However, the stability of micelles under flow induced stress is still an unknown factor. It should be noted that to confirm the breaking of micelles, the fluid must be imaged while flowing, since if the flow and therefore the shear would stop, the micelles would quickly self-assemble again such that the reassembled fluid is indistinguishable from the original.

4.2 Nanofluid characterisation

To study the mechanism affecting the heat transfer coefficient of nanofluids, it is imperative to characterize samples carefully. Important qualities are viscosity, specific heat and thermal conductivity and droplet size distribution. These are characterized using widely accepted methods such as dynamic light scattering and differential scanning calorimetry.

4.2.1 Dynamic light scattering

The size distribution of the droplets is determined by a dynamic light scattering (DLS) measurement. In a DLS measurement, a laser is directed at the

colloid studied. Light scatters randomly to all directions from small particles. As particles move due to Brownian motion, scattering intensity fluctuates. The fluctuation is correlated to the motion of the particles and the motion of particles is related to its size via the Stokes' equation for friction of a sphere moving in a viscous medium

$$F_d = -6\pi\mu R v, \tag{4.1}$$

where F_d is the frictional force, μ the viscosity, R the radius of the sphere and v its speed.

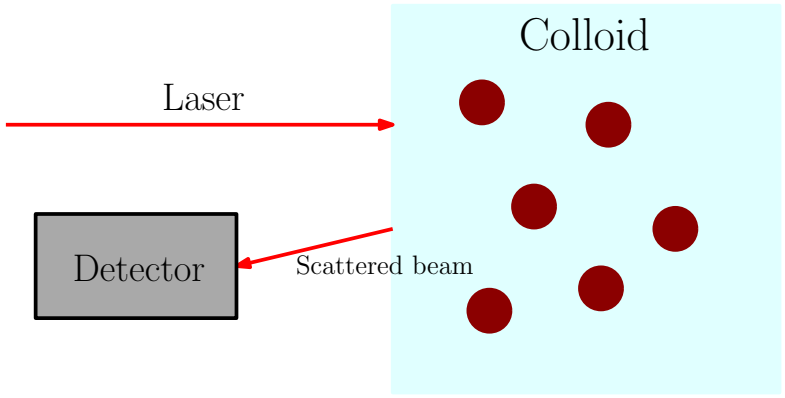

Figure 4.3: The fluctuation of the intensity of a scattered laser beam is related to the velocity of the particles which is related to the size of the particles.

4.2.2 Differential scanning calorimetry

The heat capacity of the nanofluid was measured using a differential scanning calorimetry (DSC) device. The principle of a DSC measurement is following: in the sample chamber is a reference sample and the sample we want to measure. The heat capacity of the reference and the response of a reference system consisting of an empty sample crucible and the reference sample to heating are well known. The thermal capacity is then derived from the difference in heating between the reference system and the system containing the sample.

Besides direct measurement, a well established formula [62][68] exists to calculate specific heats of two component systems

$$c_{p,nf} = \frac{\phi\rho_p c_{p,p} + (1-\phi)\rho_{bf} c_{p,bf}}{\rho_{nf}}, \tag{4.2}$$

where $c_{p,p}$ and $c_{p,bf}$ are the specific heats of the particle or droplet and the base fluid.

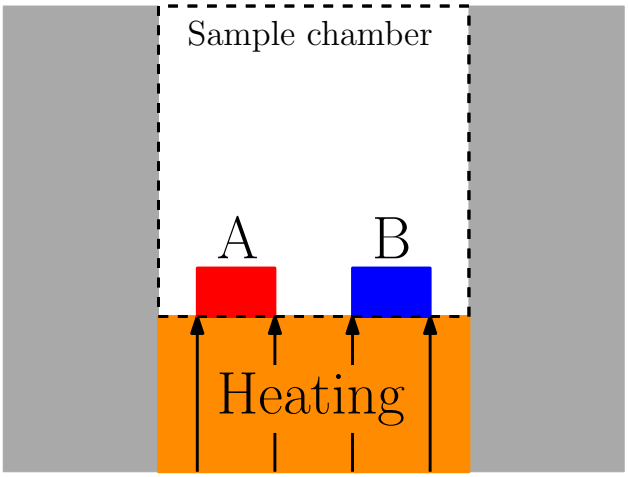

Figure 4.4: In a DSC A is the sample to be measured and B is the reference sample. Both are heated in well isolated sample chamber. The response to the heating of the sample chamber, empty measurement crucible and the reference sample are well known.

4.2.3 Thermal conductivity measurement

The thermal conductivities of the samples were measured using a modified transient plate source measurement device. Essentially, in the measurement, the sample is heated on a plate and the systems response to the heating is measured. The advantages of this method are that it is easy to use and the measurements are quick to perform. Experimentally obtained results were then compared to the the prediction of the Maxwell's formula.

4.2.4 Viscosity measurement

The viscosity of the fluid was found using a falling ball viscometer. The operating principle of it is - as the name suggests - to measure the time it takes for a ball to fall a given length in the studied substance. The viscosity is then calculated as follows

$$\mu = K(\rho_{ball} - \rho_{fluid})t, \tag{4.3}$$

where K is the ball constant given by the manufacturer of the measurement device, ρ_{ball} the density of the ball, ρ_{fluid} the density of the fluid and t the falling time.

Viscosity of a colloid that has a relatively small fraction of dispersed phase can be estimated by a formula derived exactly by Einstein in 1906 [69]

$$\mu_r = 1 + 2.5\phi, \tag{4.4}$$

where $\mu_r = \mu_{colloid}/\mu_{basefluid}$ is the relative viscosity of the colloid. However, empirical studies mentioned before indicate that the Einstein equation tends to underestimate the viscosities of nanoscale colloids. A simple approach would be to add higher order correction terms

$$\mu_r = 1 + 2.5\phi + B\phi^2 + C\phi^3 \ldots \tag{4.5}$$

and fitting the equation to the empirical data. Han and Yang used a second order correction and found that the coefficient $B = 117$ for water in FC72 nanoemulsions. We will compare this equation to the measured viscosities of the samples we have prepared.

4.3 Convective Heat transfer measurement

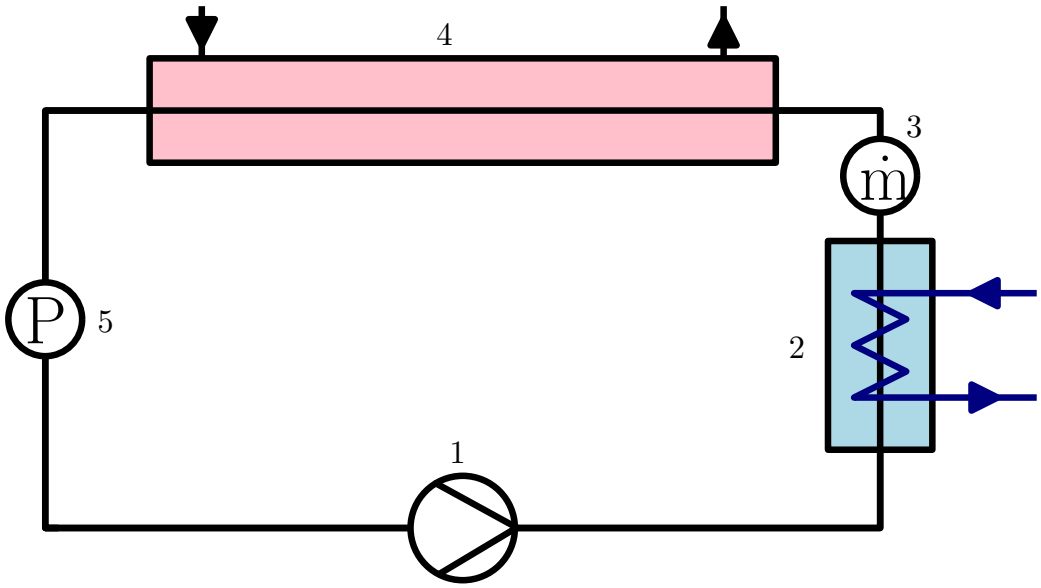

Figure 4.5: The measurement scheme for forced convective heat transfer of nanofluids. It consists of a pump (1), a heat exchanger to cool the nanofluid (2), mass flow measurement (3), a steam heat exchanger (4) and the pressure difference measurement (5).

The experimental setup is presented in figure 4.5. It consist of the closed nanofluid loop and a heat exchanger. The heat exchanger consist of a 1.5m long annular steel pipe such that the nanofluid flows inside the inner tube and saturated subatmoshperic steam flows in the outer section. The steam was chosen to be at subatmospheric pressure and thus at temperature less

than 100°C to avoid boiling of water based nanofluids. Typical pressure of the steam during measurement was 0.4 bar and the corresponding steam temperature was between 72 and 76 degrees Celcius. The heat exchanger acts as the masurement tube and the temperatures of out- and ingoing nanofluid and steam are measured at the ends of the measurement tube. Pressure losses for the length of the exchanger and the mass flow of the nanofluid are also monitored.

Earlier measurements in the laminar flow region indicate that natural convection has significant effect for a horizontal measurement tube and thus the configuration of the system was changed such that the measurement tube is vertical and the nanofluid flows upwards in the tube.

4.3.1 Calculation of the heat transfer coefficient

To determine the heat transfer coefficient, the total conductance of the heat exchanger G must be calculated from the experimental data. Total conductance is defined as

$$G = \frac{\phi}{\Theta_{ln}} = \frac{\dot{m} c_p \Delta T}{\Theta_{ln}}, \tag{4.6}$$

where $\dot{m}$ is the mass flow, c_p the heat capacity of the nanofluid, ΔT the temperature difference between incoming and outgoing fluid and Θ_{ln} the logarithmic temperature difference defined as a function of in- and outgoing temperatures of the fluid and the steam

$$\Theta_{ln} = \frac{(T_{steam,in} - T_{nano,out}) - (T_{steam,out} - T_{nano,in})}{\ln\left[\frac{(T_{steam,in} - T_{nano,out})}{(T_{steam,out} - T_{nano,in})}\right]}, \tag{4.7}$$

where $T_{i,j}$ are temperatures of steam and nanofluid.

Conductance per length is

$$\frac{1}{G'} = \frac{1}{G/L} = \frac{1}{\pi d_{in} h} + \frac{1}{\pi d_o h_0} + \frac{\ln(d_o/d_{in})}{2\pi k_{pipe}}, \tag{4.8}$$

where d_in is the diameter of the inner pipe, h the heat transfer coefficient of the test fluid, d_o the diameter of the outer pipe, h_o the heat transfer coefficient of the steam and k_{pipe} the heat conduction of the pipe. k_{pipe} was known from theoretical values and h_0 was determined by measuring the heat transfer coefficient of water and comparing the result to known correlation formulae. The heat transfer coefficient of the nanofluid is then easily solved from equation (4.8).

In the experiment, we measure the temperatures of the steam and nanofluids and the mass flow of the nanofluid. Other coefficients in the equation (4.8)

are constants of the measurement device and determined in the calibration of the system.

4.3.2 Heat transfer efficiency

Comparing pure heat transfer coefficient between the nanofluid and base fluid yields very little information. Increase in viscosity also causes an increase in the required pumping power to reach similar Reynols number regime and therefore also the efficiency must be considered.

Addition of particles or droplets in the fluid increases viscosity compared to the base fluid. Einstein's equation $\mu' = (1 + 2.5\phi)\mu_{base}$ predicts moderate increase of viscosity, but empirical studies have reported even greater increases in viscosity. This is problematic, since viscosity increases pressure losses Δp which in turn increase the required pumping power. We thus define heat transfer efficiency as the relative pumping power at constant heat transfer coefficient

$$\eta = \frac{P_{bf}(h)}{P_{nf}(h)} \tag{4.9}$$

where $P = \dot{V}\Delta p$ is the relevant pumping power at constant mass flow. Thus we can calculate the relative pumping power to the base fluid for the nanofluid as a function of h. The implications of the relative pumping power are following: it is a measure telling if the increased heat transfer could be achieved more efficiently by increasing the pumping power while keeping the original fluid instead of the nanofluid. Value larger than one is to be interpreted such that the fluid requires more power to achieve similar heat transfer coefficient than the base fluid. Previous study [70] found that for most nanofluids and small Reynolds numbers, the nanofluid is in fact less efficient as a heat transfer medium than the basedfluid. This is illustrated in figure 4.6 (It should be noted that this figure uses opposite convention where values below one mean that the nanofluid is more efficient.

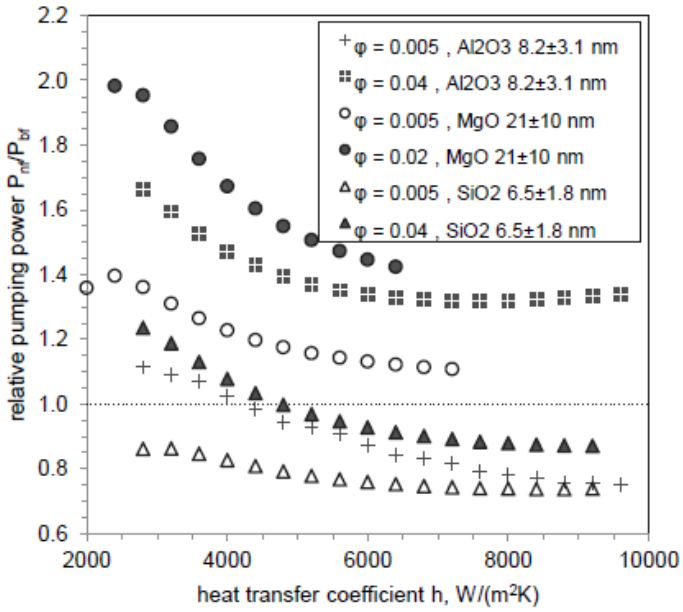

Figure 4.6: Relative pumping power for various nanofluids. [70]

Chapter 5

Results

5.1 Experimental series

For materials we chose to use N-decane as the dispersed phase, since it and similar substances such as tetradecane had been utilized successfully to prepare nanoscale emulsions in previous studies [5][71]. For surfactants we used a mixture of Sorbitane trioleate (Span 85) and Polysorbate 20 (Tween 20) to create a surfactant with optimal HLB value.

For the convective heat transfer study we chose to prepare a series of five N-decane-in-water emulsions of varying droplet fractions. The composition of the samples is shown in table 5.1. Initial optimization of emulsification parameters led to HLB value of 14 but further experiments were also carried out with a HLB value of 11. For emulsification, we used a 400W ultrasonic mixer for various times. We found that to stabilize the droplet size, large samples have to be mixed between 150 to 180 minutes using 30% pulse cycling to control heating of the sample. Emulsification of samples to nanoscale was successful using small quantities of less than 100 ml, but we were unable to reach as small droplet size on larger emulsions required for the convective heat transfer measurement despite otherwise similar composition and methods.

Additionally, during the sample preparation, we noticed that pure Tween 20 in water spontaneously forms very small agglomerates approximately of the size of 10 nm. Therefore, we also prepared three Tween 20 micelle samples. One sample was also prepared using sodium dodecyl sulfate (SDS), which also formed very small agglomerates. If Brownian motion is chiefly responsible for observed enhancements, small droplet size is naturally desirable. Previous studies using the same measurement setup observed a correlation between small particle size and good heat transfer efficiency. However, it should be noted that the form of micelles is more susceptible to perturba-

Table 5.1: Composition of test samples. The droplet column indicates the droplet material and fraction of the sample, the surfactant column has the amount of surfactant used and its HLB value and the diameter column is the average diameter of the droplets based on the number density measurement. The continuous phase in all samples is de-ionized water. The diameter numbers in parentheses marked with † correspond to values estimated from the TEM imaging.

Sample name	Dispersed phase	Surfactant	Diameter [nm]
HT1	<1% N-decane	0.35 % HLB 14	25
HT2	1% N-decane	0.5 % HLB 11	125 (18†)
HT3	2% N-decane	1.5% HLB 14	125 (80†)
HT4	3% N-decane	2% HLB 11	108 (110†)
HT5	5% N-decane	3% HLB 11	67
MC1	1 wt% Tween 20	-	6
MC2	2 wt% Tween 20	-	6
MC3	5 wt% Tween 20	-	6 (10†)
SDS	0.67 wt% SDS	-	2

tions than that of the conventional emulsion droplets meaning that under turbulent flow conditions, micelles might break or change shape significantly. Also it should be noted that the HLB-value, i.e. the hydrophilic-lipophilic-balance is a function of temperature and thus the properties of a micelle colloid might change significantly during heat transfer measurement.

As a reference, we replicated the nanofluid with best heat transfer characteristics from earlier measurements made with the same equipment we used [70], namely a 1% mass SiO_2 in water. New measurements with this sample were in good agreement with previous data.

5.2 Nanofluid characteristics

All characteristics of samples are collected in table 5.2. To find the sample composition, we urge the reader to cross reference table 5.1.

5.2.1 Size distribution

The average size data for each sample is presented in table 5.2. In figure 5.1 we see that the micelles are almost completely uniform in size. For nanoemulsions, the size distribution was less uniform, but peaks were easily identifiable. Few samples were also imaged using a cryo-TEM (see Fig. 5.2).

Table 5.2: Fluid and thermal properties of the nanofluids. The viscosities are the following: μ_m is the measured value, c_p is the specific heat and ρ the density of the fluid. The literature values for water are given for completeness.

Sample name	μ_m [mPa·s]	k_{nf}/k_{bf}	c_p [$\mathrm{Jg^{-1}K^{-1}}$]	ρ [$\mathrm{kg{\cdot}m^{-3}}$]
HT1	0.78	0.993	4.21	0.99
HT2	0.76	0.965	4.21	0.99
HT3	0.79	0.982	4.09	0.99
HT4	0.89	0.915	4.02	0.99
HT5	0.94	0.937	4.00	0.99
MC1	0.78	0.995	4.18	1.00
MC2	0.82	0.975	4.06	0.99
MC3	0.96	0.952	3.95	1.01
SDS1	0.75	1.000	4.21	1.00
Water	0.77	1.000	4.18	1.00

The size estimates obtained were generally in good agreement with the DLS data.

5.2.2 Viscosity

Surprisingly, the large nanoemulsions follow the predictions of the Einstein model with relatively good accuracy. The comparison is visualized in figure 5.3. The reason for this might be in the size distribution or the nature of emulsions as opposed to solid particles since for example clustering is a non-issue in emulsions. The second order correction was based on empirical data using very small emulsions. Our measurements indicate that no significant increase in viscosity besides Einstein model and the 2nd order correction term clearly overestimates viscosities for our samples. For small volume fraction, the measurements even indicate lower viscosity than for water, but we believe this is an artifact of the measurement, since the temperature control method was relatively crude, i.e. via ordinary water tap. However, the temperature was measured up to two decimal places and stable through the measurement but there still is uncertainty in the temperature of the sample tube and measurements made on different dates.

5.2.3 Thermal conductivity

Our measurements indicate that the emulsions follow Maxwell's formulas predictions with good accuracy as illustrated in figure 5.4. The reason for not observing any deviations might reside in the nature of our samples. The

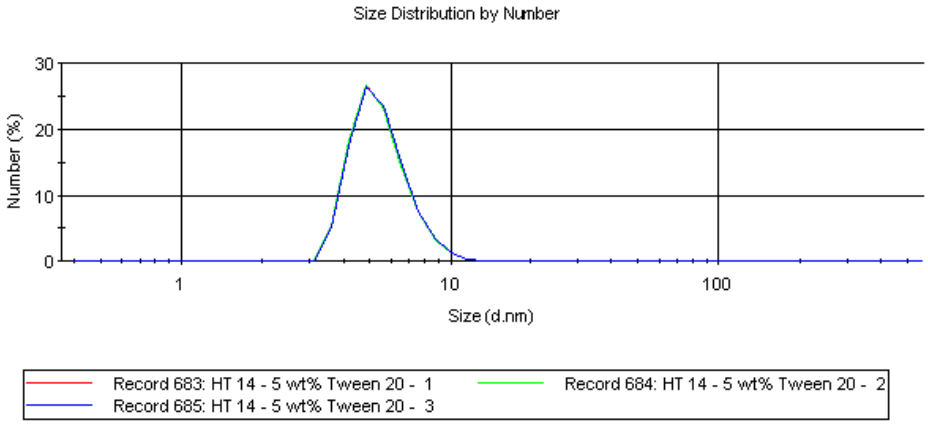

Figure 5.1: The number size distribution for 5% Tween 20 micelles in water. The distributions for three consecutive measurements are nearly identical.

droplet size in few samples was relatively large, near 100 nm, which would put the samples at the upper end of the size scale of nanoparticles.

5.2.4 Specific heat

The specific heat of water is well known and thus its measurement was omitted, except to verify the accuracy of the measurement device, and the literature value was used in calculations. A result of a typical DSC-measurement curve is presented in figure 5.5. The actual specific heats of the samples are presented in table 5.2. The values for the emulsions and micelle samples are lower than the specific heat of the basefluid as expected since both n-decane and the surfactants have lower specific heats than water.

5.3 Heat transfer coefficients

5.3.1 Measurement calibration

Since the measurement scheme has underwent a few changes after the previous sample series, new calibration had to be made to obtain a baseline against which to compare the heat transfer of nanoemulsions. Water is very useful in this role as it is readily available and its properties are well documented and it is also the basefluid of choice.

The important value to be calibrated was the heat transfer coefficient of the subatmospheric steam h_0 since other constants of the system were well known. In the calibration, multiple measurements with water were made

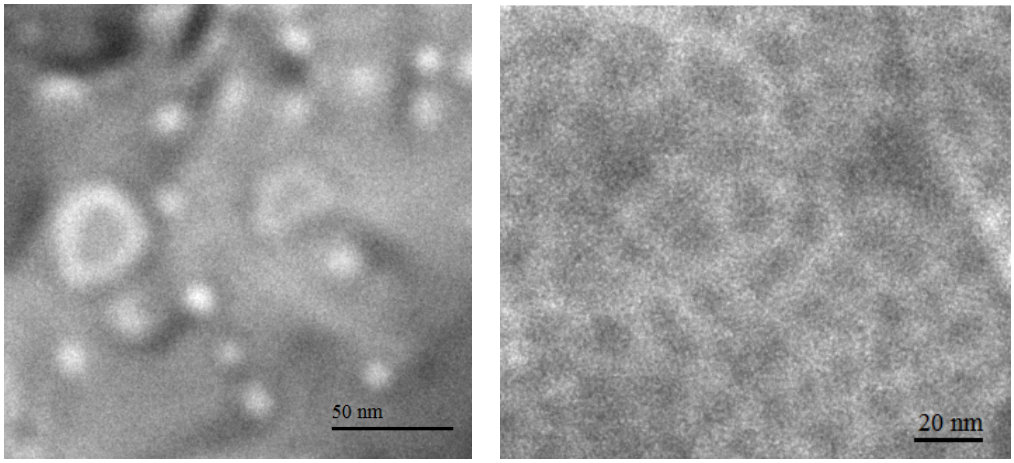

(a) Image of the sample HT2 (b) Image of the sample MC5

Figure 5.2: Size distributions based on TEM images agree well with the DLS measurements.

and the result was compared to the Hausen [72] and Sieder-Tate [73] correlations. The correlations were in good agreement with the measurements when $h_0 \approx 9kW/Km^2$. It should be noted that the correlations are empirical approximations and thus the values obtained using them are not exact. However, the measurements were highly repeatable and thus the relative heat transfer coefficient h_{nano}/h_{base} should be relatively accurate. In repeated water measurements, the deviation was on average 5% or less for the range of Reynolds numbers used.

5.3.2 Heat transfer measurements

The heat transfer data is presented in figures 5.7 and 5.6. As can be readily seen, fluids with higher droplet loading and higher viscosity exhibit higher heat transfer coefficient for equal Reynolds number. Furthermore, based on the measurements, the increase in heat transfer coefficient is proportionally larger at the largest Reynolds number values. Unfortunately, the current equipment was insufficient to reach the regime of Re $>$ 10000. Ultimately, there is very little information concerning the heat transfer capabilities of the samples to be gathered from the heat transfer coefficient only.

5.3.3 Heat transfer efficiency

Based on the pressure loss data, we can calculate the relative pumping power $P_\eta = P_{bf}(h_1)/P_{nf}(h_1)$, where h_1 is a constant heat transfer coefficient. Pump-

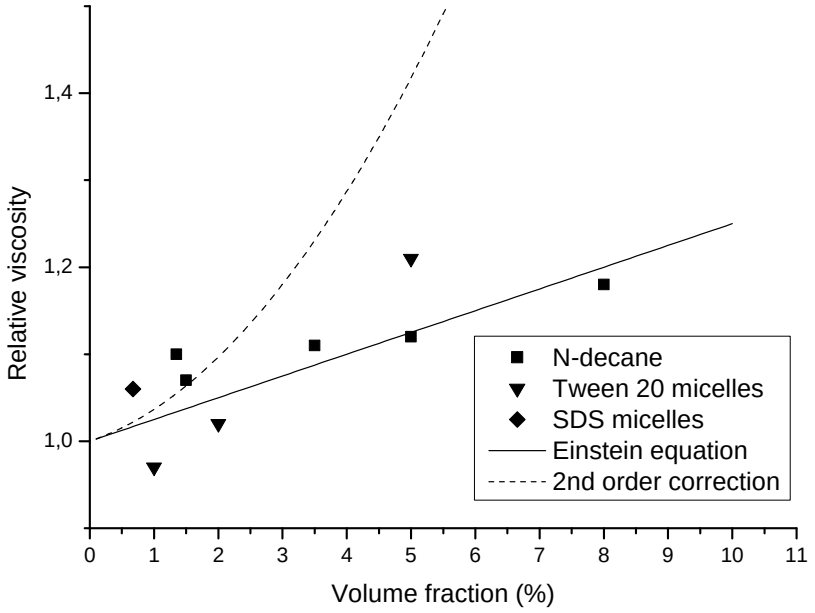

Figure 5.3: Viscosities of emulsions compared to the estimates of Einstein's model and the Einstein model with second order correction term.

ing efficiencies are illustrated in figure 5.8. As we can see, the low efficiency correlates with high droplet loading and larger particles size and conversely efficiencies near unity correspond to samples with low volume fraction of droplets and small particle size. These findings coincide with results obtained previously for solid particle nanofluids using the same measurement setup [70].

5.3.4 Nusselt number

The Nusselt number is the relation between convective and conductive heat transfer. Using the formula defined in chapter 3, where the characteristic length of the system in the case of the pipe flow is the diameter of the pipe, we can calculate the Nusselt number for all samples besides the SDS-micelle sample for which the thermal conductivity data was unavailable. The results are illustrated in figures 5.9 and 5.10.

As the thermal conductivity of the samples relative to the basefluid was typically less than unity, the Nusselt number should increase compared to the data for the heat transfer coefficient, and such increase was indeed observed.

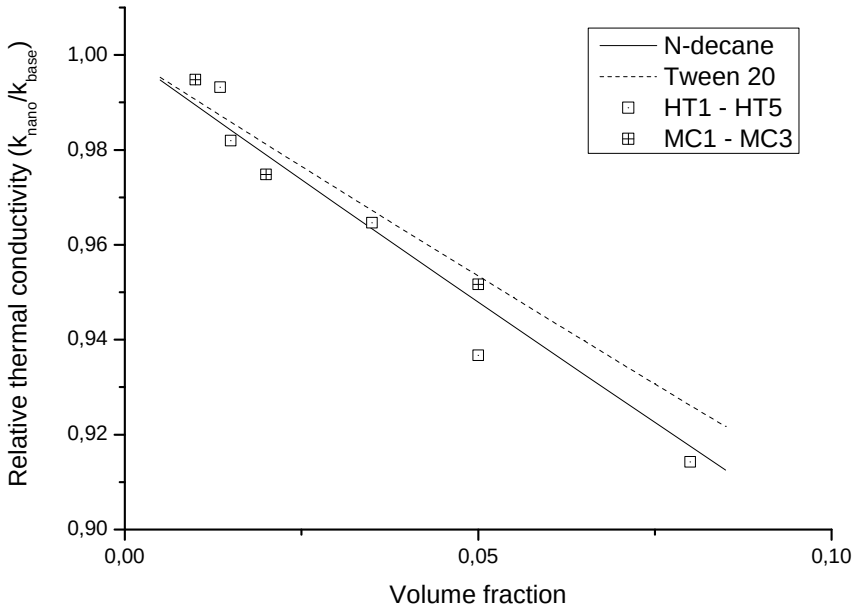

Figure 5.4: Thermal conductivities of the samples compared to the prediction of the Maxwell's formula.

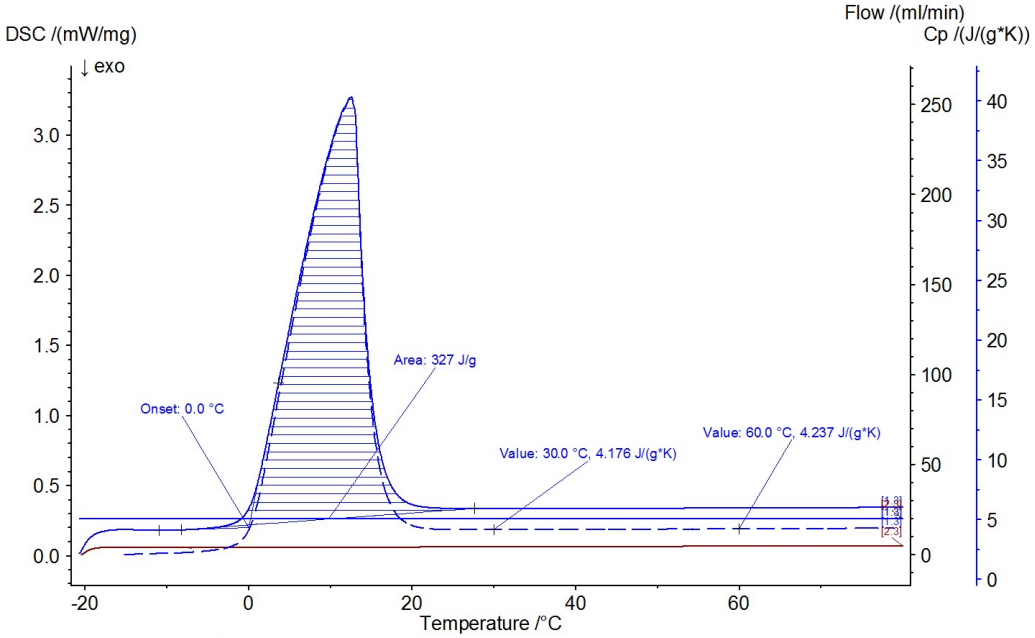

Figure 5.5: A typical DSC-curve for heat capacity measurement result. The figure is for 1 mass% Tween 20 micelles in water solution.

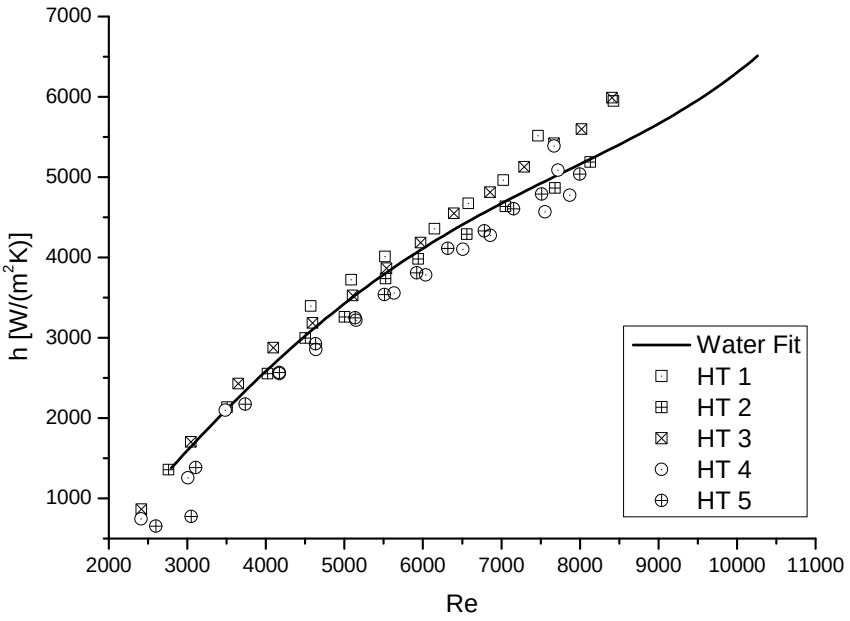

Figure 5.6: The heat transfer coefficient h of n-decane as a function of the Reynolds number Re.

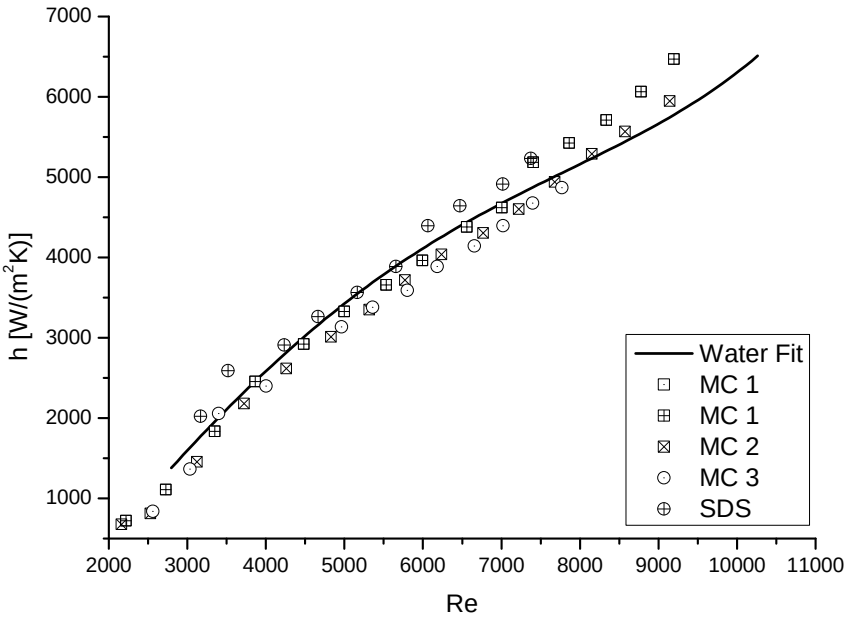

Figure 5.7: The bare heat transfer coefficient h of micelle samples as a function of the Reynolds number Re.

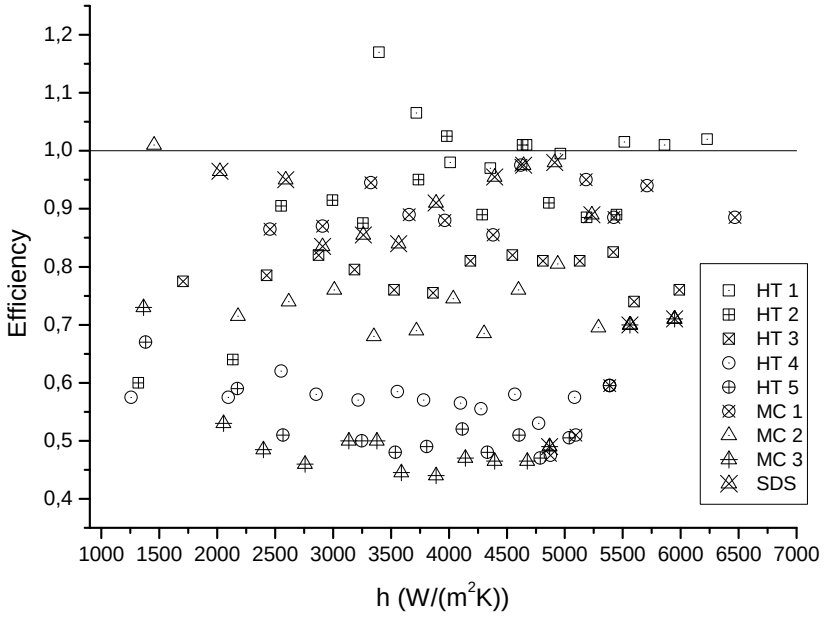

Figure 5.8: The heat transfer efficiency of the studied samples.

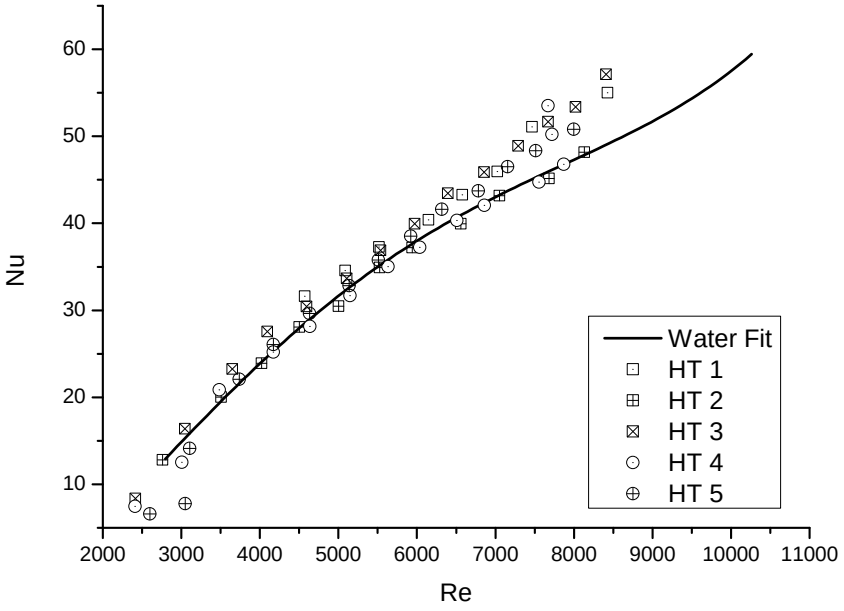

Figure 5.9: The Nusselt number of n-decane emulsions.

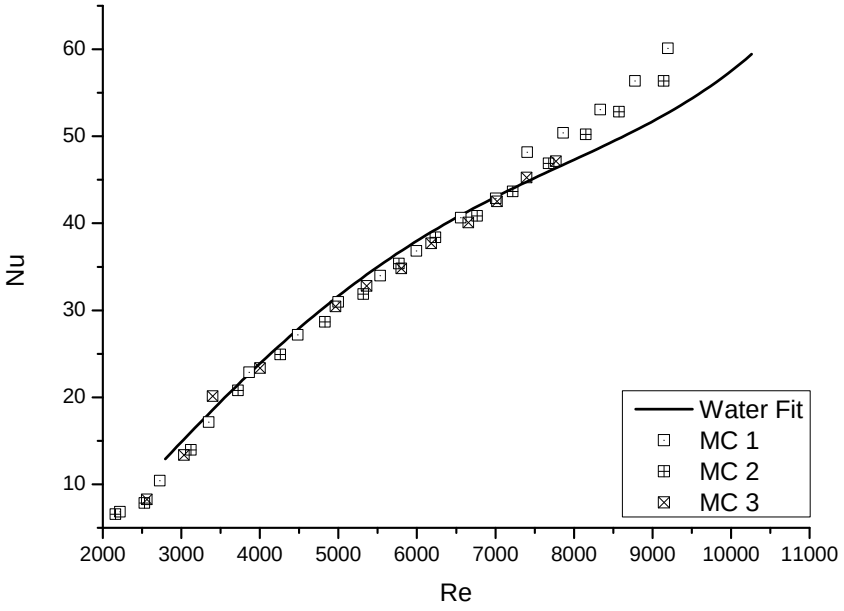

Figure 5.10: The Nusselt number of the micelles.

Chapter 6

Conclusions and discussion

6.1 Thermal conductivity

The theory of thermal conductivity in the solid particle nanofluids is still a controversial subject. No conclusive evidence has been presented to completely rule out different proposals. However, parallels between nanoemulsions and nanofluids might provide insight into different mechanisms. Both clustering and liquid layering theories require that the dispersed phase consists of solid particles and within certain assumptions they could produce effects comparable to the experimental results. However, Brownian motion does not require specific assumptions about the material or the structure of the particles, and thus would in that sense be an elegant solution. Still, nature does not care about beauty and further inquiry to thermal conductivity of nanofluids is certainly necessary to solve the conundrum.

In our experiments however, we saw no diversion from the Maxwell's formula. It might be still too early to draw conclusions based on this dataset and a new sample series with smaller droplet sizes or different materials to verify our findings would be useful. Nevertheless, if the trend continues with further experiments using the same experimental apparatus, either the "new physics" solutions or the reliability of the experiments must be questioned.

6.2 Convection

The bulk of our experimental work was directed to the measurement of convective heat transfer coefficient. During the optimization of the samples, we successfully prepared nanoscale samples with different volume fractions of droplets. However, we were unable to emulsify larger samples to such small size scale. One reason might be that the ultrasonic mixer is of inadequate

power. Our understanding of parameters having an effect on emulsification is still incomplete. Further problem concerning the preparation process is that each substance pair of continuous and dispersed phase must be separately optimized. Indeed, multiple studies have only considered the preparation process.

However, the turbulent heat transfer measurements have novelty value. There is very little literature on convective heat transfer of nanoemulsions, especially in the turbulent region. Our findings indicate that relatively large, meaning diameters of the order 100 to 150 nm, emulsions have little advantage over the base fluid in the Reynolds number range 2000 to 8000. This mirrors previous experiments done on the same measurement device [70], where the heat transfer coefficient increased but the overall efficiency was worse for all but the smallest particles. The efficiencies of our samples followed a similar trend.

Perhaps the most interesting part of the experimental series is the increase in the Nusselt number. The increase compared to the heat transfer coefficient is only natural in light of the thermal conductivity data. However, it is curious that all the qualities of the samples were worse from the point of view of convective applications, yet the heat transfer coefficients and Nusselt numbers were comparable or higher than the basefluid.

6.3 Directions for future research

While first results are less than revolutionary, additional measurements using nanoemulsions of smaller droplet size would be of great interest. This would require further optimization of preparation of large samples of volumes >1500 ml. If the current ultrasonic mixer indeed is ineffective, low energy emulsification methods, such as phase inversion temperature method, should be investigated.

Besides smaller emulsions, another interesting direction would be phase-change materials. The latent heat associated with melting and solidification is usually very large and if materials would be chosen such that their melting point is suitable for the system, i.e. between the coolest and warmest temperature in the cycle, this energy release could be harnessed.

Acknowledgments

This thesis was part of the EFEU project funded by Strategic Centre of Science, Technology and Innovation (Cleen Ltd.), Nanofluid project funded by Academy of Finland, and EXPECTS project funded by Aalto Energy Efficiency Program.

I would also like to thank dr. Ari Seppälä for supervising the thesis and for offering an interesting research problem to work with. Additionally I thank Salla Puupponen for help with the measurements.

Bibliography

[1] Carl L. Yaws. *Chemical properties handbook*. McGraw-Hill, 1999.

[2] J. C. Maxwell. *A Treatise on Electricity and Magnetism*, volume 1. 1873.

[3] Z.H. Han and B. Yang. Thermophysical characteristics of water-in-fc72 nanoemulsion fluids. *Appl. Phys. Lett.*, 92, 2008.

[4] B. Yang and Z.H. Han. Thermal conductivity enhancement in water-in-fc72 nanoemulsion fluids. *Appl. Phys. Lett.*, 88, 2006.

[5] Hea Youn Sul, Hiki Hong, and Yong Tae Kang. Thermal conductivity measurement of oil in water (o/w) nanoemulsion and oil in h_2o/libr (o/s) binary nanoemulsion for absorption application. *International Journal of Refrigeration*, 34:1360–1365, 2011.

[6] *ISI Web of Knowledge 20.9.2013*.

[7] P Keblinski, S.R Phillpot, S.U.S Choi, and J.A Eastman. Mechanisms of heat flow in suspensions of nano-sized particles (nanofluids). *International Journal of Heat and Mass Transfer*, 45(4):855 – 863, 2002.

[8] Pawel Keblinski, Ravi Prasher, and Jacob Eapen. Thermal conductance of nanofluids: is the controversy over? *Journal of nanoparticle reseach*, 10:1089–1097, 2008.

[9] Sarit Kumar Das, Stephen U. S. Choi, and Hrishikesh E. Patel. Heat transfer in nanofluids: A review. *Heat Transfer Engineering*, 27(10):3–19, 2006.

[10] S.M.S. Murshed, K.C. Leong, and C. Yang. Thermophysical and electrokinetic properties of nanofluids: A critical review. *Applied Thermal Engineering*, 28:2109 – 2125, 2008.

[11] Joseph Fourier. *Théorie analytique de la chaleur*. 1822.

[12] R. L. Hamilton and O. K. Crosser. Thermal conductivity of heterogeneous two-component systems. *Industrial & Engineering Chemistry Fundamentals*, 1(3):187–191, 1962.

[13] J. C. Maxwell Garnett. Colours in metal glasses, in metallic films and in metallic solutions. *Proceedings of the Royal Society of London*, 76, 1905.

[14] Z. Hashin and S. Shtrikman. A variational approach to the theory of the elastic behaviour of multiphase materials. *Journal of the Mechanics and Physics of Solids*, 11(2):127 – 140, 1963.

[15] S. M. Sohel Murshed. Correction and comment on "thermal conductance of nanofluids: is the controversy over?". *Journal of nanoparticle reseach*, 11:511–512, 2009.

[16] Tae-Keun Hong, Ho-Soon Yang, and C.J. Choi. Study of the enhanced thermal conductivity of fe nanofluids. *Journal of Applied Physics*, 97, 2005.

[17] S. U. S. Choi, Z. G. Zhang, W. Yu, F. E. Lockwood, and E. A. Grulke. Anomalous thermal conductivity enhancement in nanotube suspensions. *Applied Physics Letters*, 79(14):2252–2254, 2001.

[18] Sarit Kumar Das, Nandy Putra, Peter Thiesen, and Wilfried Roetzel. Temperature dependence of thermal conductivity enhancement for nanofluids. *Journal of Heat Transfer*, 125:567–574, 2003.

[19] Jacob Eapen, Roberto Rusconi, Roberto Piazza, and Sidney Yip. The classical nature of thermal conduction in nanofluids. *arXiv:0901.0058 [cond-mat.soft]*.

[20] Hyun Uk Kang, Sung Hyun Kim, and Je Myung Oh. Estimation of thermal conductivity of nanofluid using experimental effective particle volume. *Experimental Heat Transfer*, 19(3):181–191, 2006.

[21] S. Lee, S. U.-S. Choi, S. Li, and J. A. Eastman. Measuring thermal conductivity of fluids containing oxide nanoparticles. *Journal of Heat Transfer*, 121(2):280–289, May 1999.

[22] Calvin H. Li and G. P. Peterson. Experimental investigation of temperature and volume fraction variations on the effective thermal conductivity of nanoparticle suspensions (nanofluids). *Journal of Applied Physics*, 99(8):084314, 2006.

[23] J. A. Eastman, U. S. Choi, S. Li, L. J. Thompson, and S. Lee. Enhanced thermal conductivity through the development of nanofluids. *MRS Proceedings*, 457, 1 1996.

[24] Y. Hwang, J.K. Lee, C.H. Lee, Y.M. Jung, S.I. Cheong, C.G. Lee, B.C. Ku, and S.P. Jang. Stability and thermal conductivity characteristics of nanofluids. *Thermochimica Acta*, 455:70 – 74, 2007.

[25] J. A. Eastman, S. U. S. Choi, S. Li, W. Yu, and L. J. Thompson. Anomalously increased effective thermal conductivities of ethylene glycol-based nanofluids containing copper nanoparticles. *Applied Physics Letters*, 78(6):718–720, 2001.

[26] S.M.S. Murshed, K.C. Leong, and C. Yang. Enhanced thermal conductivity of tio2 - water based nanofluids. *International Journal of Thermal Sciences*, 44(4):367 – 373, 2005.

[27] S M S Murshed, K C Leong, and C Yang. Determination of the effective thermal diffusivity of nanofluids by the double hot-wire technique. *Journal of Physics D: Applied Physics*, 39(24):5316, 2006.

[28] G. H. Geiger and D. R. Poirier. *Tranport phenomena in metallurgy*. Addison-Wesley, 1973.

[29] X. Wang, X. Xu, and S. U. S. Choi. Thermal conductivity of nanoparticle-fluid mixture. *J Thermophys Heat Transfer*, 13(4):474–480, 1999.

[30] Bock Choon Pak and Young I. Cho. Hydrodynamic and heat transfer study of dispersed fluids with submicron metallic oxide particles. *Experimental Heat Transfer*, 11(2):151–170, 1998.

[31] J.R. Henderson and F. van Swol. On the interface between a fluid and a planar wall. *Molecular Physics*, 51(4):991–1010, 1984.

[32] Huaqing Xie, Motoo Fujii, and Xing Zhang. Effect of interfacial nanolayer on the effective thermal conductivity of nanoparticle-fluid mixture. *International Journal of Heat and Mass Transfer*, 48(14):2926 – 2932, 2005.

[33] W. Yu and S.U.S. Choi. The role of interfacial layers in the enhanced thermal conductivity of nanofluids: A renovated maxwell model. *Journal of Nanoparticle Research*, 5:167–171, 2003. 10.1023/A:1024438603801.

[34] P.L. Kapitza. *J. Phys (USSR)*, 4, 1941.

[35] J.A. Eastman, S.R. Phillpot, S.U.S. Choi, and P. Keblinski. Thermal transport in nanofluids. *Annual Review of Materials Research*, 34(1):219–246, 2004.

[36] Seok Pil Jang and Stephen U. S. Choi. Effects of various parameters on nanofluid thermal conductivity. *Journal of Heat Transfer*, 129:617 – 623, 2006.

[37] *Numerical study of the effective Thermal conductivity of nanofluids*, Proceedings of HT 2005 2005 ASME Summer Heat Transfer Conference July 17-22, 2005, San Francisco, California, USA.

[38] Gianluca Puliti, Samuel Paolucci, and Mihir Sen. Thermodynamic properties of gold-water nanofluids using molecular dynamics. *Journal of Nanoparticle Research*, 14:1296, 2012.

[39] Ling Li, Yuwen Zhang, Hongbin Ma, and Mo Yang. An investigation of molecular layering at the liquid-solid interface in nanofluids by molecular dynamics simulation. *Physics Letters A*, 372:4541 – 4544, 2008.

[40] Thomas C. Hales. An overview on the kepler conjecture. *arXiv:math/9811071 [math.MG]*, 1998.

[41] Sang Hyun Kim, Sun Rock Choi, and Dongsik Kim. Thermal conductivity of metal-oxide nanofluids: Particle size dependence and effect of laser irradiation. *Journal of Heat Transfer*, 129(3):298–307, May 2006.

[42] William Evans, Ravi Prasher, Jacob Fish, Paul Meakin, Patrick Phelan, and Pawel Keblinski. Effect of aggregation and interfacial thermal resistance on thermal conductivity of nanocomposites and colloidal nanofluids. *International Journal of Heat and Mass Transfer*, 51:1431 – 1438, 2008.

[43] Yongjin Feng, Boming Yu, Peng Xu, and Mingqing Zou. The effective thermal conductivity of nanofluids based on the nanolayer and the aggregation of nanoparticles. *Journal of Physics D: Applied Physics*, 40:3164, 2007.

[44] John Philip, P D Shima, and Baldev Raj. Evidence for enhanced thermal conduction through percolating structures in nanofluids. *Nanotechnology*, 19, 2008.

[45] Ravi Prasher, Patrick E. Phelan, and Prajesh Bhattacharya. Effect of aggregation kinetics on the thermal conductivity of nanoscale colloidal solutions (nanofluid). *Nano Letters*, 6:1529 – 1534, 2006.

[46] K. S. Hong andTae Keun Hong and Ho-Soon Yang. Thermal conductivity of fe nanofluids depending on the cluster size of nanoparticles. *Applied Physics Letters*, 88, 2006.

[47] N.R. Karthikeyan, John Philip, and Baldev Raj. Effect of clustering on the thermal conductivity of nanofluids. *Materials Chemistry and Physics*, 109:50 – 55, 2008.

[48] Dae-Whang Yoo, K.S. Hong, T.E. Hong, J.A. Eastman, and Ho-Soon Yang. Thermal sonductivity of al_2o_3/water nanofluids. *Journal of the Korean Physical Society*, 51:84 – 87, 2007.

[49] J.A. Eastman, U.S. Choi, S. Li, G. Soyez, L.J. Thompson, and R.J. DiMelfi. Novel thermal properties of nanostructured materials. *Journal of Metastable and Nanocrystallinen Materials*, 2 - 6:629, 1999.

[50] Robert Brown. A brief account of microscopical observations made in the months of june, july and august, 1827, on the particles contained in the pollen of plants; and on the general existence of active molecules in organic and inorganic bodies. *Philosophical Journal*, 4:161–173, 1828.

[51] A Einstein. Über die von der molekularkinetischen theorie der wärme geforderte bewegung von in ruhenden flüssigkeiten suspendierten teilchen. *Annalen der Physik*, 322, 1905.

[52] P. Langevin. On the theory of brownian motion. *C. R. Acad. Sci. (Paris)*, 146:530 – 533, 1908.

[53] Junemoo Koo and Clement Kleinstreuer. A new thermal conductivity model for nanofluids. *Journal of nanoparticle reseach*, 6:577–588, 2005.

[54] Seok Pil Jang and Stephen U. S. Choi. Role of brownian motion in the enhanced thermal conductivity of nanofluids. *Applied Physics Letters*, 84(21):4316–4318, 2004.

[55] Ravi Prasher, Prajesh Bhattacharya, and Patrick E. Phelan. Thermal conductivity of nanoscale colloidal solutions (nanofluids). *Phys. Rev. Lett.*, 94:025901, Jan 2005.

[56] Ravi Prasher, Prajesh Bhattacharya, and Patrick E. Phelan. Brownian-motion-based convective-conductive model for the effective thermal conductivity of nanofluids. *J. Heat Transfer.*, 128(6):588–595. doi:10.1115/1.2188509., 2005.

[57] Ratnesh K. Shukla and Vijay K. Dir. Effect of brownian motion on thermal conductivity of nanofluids. *Journal of Heat Transfer*, 130, 2008.

[58] Theodore L. Bergman, Adrienne S. Lavine, Frank P. Incopera, and David P. DeWitt. *Fundamentals of Heat and Mass Transfer.* John Wiley & Sons, 2011.

[59] http://scienceworld.wolfram.com/biography/lamb.html. Cited 10.12.2013.

[60] Stephen B. Pope. *Turbulent Flows.* Cambridge University Press, 2000.

[61] Yimin Xuan and Qiang Li. Investigation on convective heat transfer and flow features of nanofluids. *Journa of Heat Transfer*, 125:151 – 155, 2003.

[62] Bak Choon Pak and Young I. Cho. Hydrodynamic and heat transfer study of dispersed fluids with submicron metallic oxide particles. *Experimental Heat Transfer*, 11:151 – 170, 1998.

[63] Sidi El Bacaye Maiga, Cong Tam Nguyen, Nicolas Galanis, and Gilles Roy. Heat transfer behaviours of nanofluids in a uniformly heated tube. *Superlattices and Microstructures*, 35(36):543 – 557, 2004.

[64] J. Buongiorno. Convective transport in nanofluids. *Journal of Heat Transfer*, 128(3):240–250, 2006. cited By (since 1996) 345.

[65] J.M. Gutiérrez, C. González, A. Maestro, I. Solè, C.M. Pey, and J. Nolla. Nano-emulsions: New applications and optimization of their preparation. *Curr. Opin. Colloid Interface Sci.*, 13:245–251, 2008.

[66] C. Solans, P. Izquierdo, J. Nolla, N. Azemar, and M.J. Garcia-Celma. Nano-emulsions. *Curr. Opin. Colloid Interface Sci.*, 10:102–110, 2005.

[67] T.G. Mason, J.N. Wilking, K. Meleson, C.B. Chang, and S.M. Graves. Nanoemulsions: formation structures and physical properties. *J. Phys.: Condens. Matter*, 18:R635–R666, 2006.

[68] Yimin Xuan and Wilfried Roetzel. Conceptions for heat transfer correlation of nanofluids. *International Journal of Heat and Mass Transfer*, 43:3701 – 3707, 2000.

[69] A. Einstein. A new determination of molecular dimensions. *Annalen der Physik*, 19:371–381, 1906.

[70] Arttu Meriläinen, Ari Seppälä, Kari Saari, Jani Seitsonen, Janne Ruokolainen, Sakari Puisto, Niko Rostedt, and Tapio Ala-Nissilä. Influence of particle size and shape on turbulent heat transfer characteristics and pressure losses in water-based nanofluids. *International Journal of Heat and Mass Transfer*, 61(0):439 – 448, 2013.

[71] P. Schalbart, M. Kawaji, and K. Fumoto. Formation of tetradecane nanoemulsion by low-energy emulsification methods. *International Journal of Refrigeration*, 33:1612–1624, 2010.

[72] H. Hausen. Darstellung des wärmeuberganges in rohren durch verallgemeinerte potenzbeziehungen. *Beih. Verfahrenstech.*, 4:91–98, 1943.

[73] E.N. Sieder and G.E. Tate. Heat transfer and pressure drop of liquids in tubes. *Ind. Eng. Chem.*, 28:1429 – 1435, 1936.